


YY1 complex in M2 macrophage promotes prostate cancer progression by upregulating IL-6

Saisai Chen,^{1,2} Kai Lu,^{1,2} Yue Hou,³ Zonghao You,^{1,2} Chuanjun Shu,⁴ Xiaoying Wei,⁵ Tiange Wu,^{1,2} Naipeng Shi,^{1,2} Guangyuan Zhang,^{1,2} Jianping Wu,^{1,2} Shuqiu Chen,^{1,2} Lihua Zhang,⁵ Wenchao Li,^{1,2} Dingxiao Zhang,⁶ Shenghong Ju,⁷ Ming Chen,^{1,2} Bin Xu ^{1,8}

To cite: Chen S, Lu K, Hou Y, et al. YY1 complex in M2 macrophage promotes prostate cancer progression by upregulating IL-6. *Journal for ImmunoTherapy of Cancer* 2023;11:e006020. doi:10.1136/jitc-2022-006020

► Additional supplemental material is published online only. To view, please visit the journal online (<http://dx.doi.org/10.1136/jitc-2022-006020>).

SC, KL, YH, ZY and CS contributed equally.

Accepted 27 March 2023



© Author(s) (or their employer(s)) 2023. Re-use permitted under CC BY-NC. No commercial re-use. See rights and permissions. Published by BMJ.

For numbered affiliations see end of article.

Correspondence to

Dr Bin Xu; njxbseu@seu.edu.cn

Dr Wenchao Li;
wenchao.li@seu.edu.cn

Professor Dingxiao Zhang;
zdx1980@hnu.edu.cn

Professor Shenghong Ju;
jsh0836@hotmail.com

Professor Ming Chen;
mingchen0712@seu.edu.cn

ABSTRACT

Background Tumor-associated macrophages are mainly polarized into the M2 phenotype, remodeling the tumor microenvironment and promoting tumor progression by secreting various cytokines.

Methods Tissue microarray consisting of prostate cancer (PCa), normal prostate, and lymph node metastatic samples from patients with PCa were stained with Yin Yang 1 (YY1) and CD163. Transgenic mice overexpressing YY1 were constructed to observe PCa tumorigenesis. Furthermore, *in vivo* and *in vitro* experiments, including CRISPR-Cas9 knock-out, RNA sequencing, chromatin immunoprecipitation (ChIP) sequencing, and liquid–liquid phase separation (LLPS) assays, were performed to investigate the role and mechanism of YY1 in M2 macrophages and PCa tumor microenvironment.

Results YY1 was highly expressed in M2 macrophages in PCa and was associated with poorer clinical outcomes. The proportion of tumor-infiltrated M2 macrophages increased in transgenic mice overexpressing YY1. In contrast, the proliferation and activity of anti-tumoral T lymphocytes were suppressed. Treatment targeting YY1 on M2 macrophages using an M2-targeting peptide-modified liposome carrier suppressed PCa cell lung metastasis and generated synergistic anti-tumoral effects with PD-1 blockade. IL-4/STAT6 pathway regulated YY1, and YY1 increased the macrophage-induced PCa progression by upregulating IL-6. Furthermore, by conducting H3K27ac-ChIP-seq in M2 macrophages and THP-1, we found that thousands of enhancers were gained during M2 macrophage polarization, and these M2-specific enhancers were enriched in YY1 ChIP-seq signals. In addition, an M2-specific IL-6 enhancer upregulated IL-6 expression through long-range chromatin interaction with IL-6 promoter in M2 macrophages. During M2 macrophage polarization, YY1 formed an LLPS, in which p300, p65, and CEBPB acted as transcriptional cofactors.

Conclusions Phase separation of the YY1 complex in M2 macrophages upregulated IL-6 by promoting IL-6 enhancer–promoter interactions, thereby increasing PCa progression.

BACKGROUND

Prostate cancer (PCa) is the second most frequently diagnosed cancer among men

WHAT IS ALREADY KNOWN ON THIS TOPIC

⇒ Studies have reported the role of Yin Yang 1 (YY1) in regulating the inflammatory factors and tissue remodeling function of macrophages. However, there is still a lack of *in vivo* verification of the function and mechanism of YY1 in transgenic mice.

WHAT THIS STUDY ADDS

⇒ Herein, we demonstrated the role of YY1 in M2 macrophages in transgenic mice overexpressing YY1 and investigated the therapeutic potential of targeting M2 macrophage YY1 to treat prostate cancer (PCa). In addition, we reported that YY1 promoted IL-6 transcription in macrophages by regulating phase separation and enhancer–promoter interactions, thus remodeling the tumor microenvironment.

HOW THIS STUDY MIGHT AFFECT RESEARCH, PRACTICE OR POLICY

⇒ These findings may lead to the development of novel therapies for PCa by targeting YY1 in prostate tumor-associated macrophages.

worldwide.¹ PCa accounts for a quarter of diagnosed cancer cases, with the second highest mortality rate in the USA.^{1,2} Due to a lack of obvious symptoms at the initial stages, approximately 20% of the patients with PCa are diagnosed with advanced disease, resulting in distant metastasis and death.¹ Androgen deprivation therapy (ADT) is effective in the initial treatment of PCa. However, most patients develop castration resistance within 2 years, followed by ADT failure.³ Immune checkpoint inhibitors (ICIs) have remarkable efficacy in some tumor types, but still their activity in PCa is limited, mainly due to the immunosuppressive tumor microenvironment (TME).⁴ Hence, the short-lived duration of these treatments and the inability to benefit a specific subset of patients with advanced PCa highlight an urgent need to explore new therapeutic strategies.



TME is a complex ecosystem that includes tumor cells, immune cells, cytokines, and stroma components and regulates the establishment of tumors.⁵ The absence of anti-tumor T lymphocytes and infiltration of macrophages are important features of the immunosuppressive TME of PCa.⁶ Macrophage is one of the most abundant components of TME, accounting for 30–50% of all infiltrated inflammatory cells.^{7–9} Macrophages can be polarized into classically activated M1-type and alternatively activated M2-type under different cytokines and growth factors, including interleukin-4 (IL-4), IL-13, and interferon- γ (IFN- γ).^{9,10} Most tumor-associated macrophages (TAMs) share similar markers, including CD206, CD163, IL-10, arginase-1 (Arg1), and the M2 subtype is widely recognized as the major phenotype in tumor-promoting TAMs (pTAMs).¹¹ pTAMs are one of the drivers of immunosuppressive TME, thus expediting malignant proliferation and metastasis.^{11,12} Macrophages have attracted attention as a promising immunotherapy target in “cold” tumors because of the close association between the immunosuppressive microenvironment and ICI unresponsiveness.¹³ However, in different tumor entities or individuals, macrophages have significant functional diversity according to diverse TME and genetic differences, which is a barrier in targeting macrophages directly.^{14,15} Therefore, in-depth mechanistic study on tumor-infiltrated M2 macrophages in specific tumor entities is instrumental in developing new approaches for immunotherapy.

Yin Yang 1 (YY1), a C2H2 zinc finger nuclear transcription factor (TF) with high evolutionary conservation, regulates approximately 7% of human genes¹⁶ and exerts multiple cellular mechanisms in tumors, including DNA repair, cell proliferation, apoptosis, cellular metabolism, epigenetic modification, microenvironment remodeling, and immune evasion.^{17–22} In PCa, YY1 is expressed on luminal, malignant, and stromal cells.²³ We previously reported that YY1 inhibits a tumor-suppressor miRNA by interacting with EZH2, thereby promoting PCa cell proliferation.²⁴ By analyzing clinical samples, we also found that YY1 was highly expressed in CD163⁺ M2 macrophages and positively correlated with the infiltration of M2 macrophages in PCa. The infiltration of YY1 highly expressing M2 macrophages led to a worse prognosis. Although some studies have indicated that YY1 is expressed on tissue-infiltrating macrophages, most have focused on inflammatory process.^{25–28} Therefore, the detailed mechanism by which YY1 regulates macrophage function in TME remains poorly understood.

Certain enhancer-enriched transcription factors, including bromodomain containing 4 (BRD4) and octamer-binding transcription factor 4 (Oct4), can form transcriptional complexes with multiple cofactors and facilitate the transcriptional process by forming phase separation condensates, thus maximizing the activation of downstream gene transcription.^{29,30} Here, we found that YY1 contains the intrinsically disordered regions (IDRs) required for phase separation. YY1 was identified as a structural regulator in the enhancer–promoter loops,³¹

suggesting that YY1 can potentially promote downstream gene transcription through the enhancer and phase separation mechanisms. However, the mechanism by which YY1 promotes enhancer–promoter loops and its role in M2 macrophage function have not been fully elucidated.

This study demonstrated that IL-4/STAT6 signaling pathway upregulated YY1 during M2 macrophage polarization, and the YY1 complex-mediated liquid–liquid phase separation (LLPS), in which p300, p65, and CEBPB were coactivators, promoted IL-6 expression in macrophages. Furthermore, YY1 increased macrophage-induced PCa progression by upregulating IL-6 and suppressing T-lymphocyte activity. An M2-specific IL-6 enhancer promoted long-range regulation of the YY1 complex on IL-6. This study provides the first insight into LLPS in macrophage function and highlights a novel role of YY1 in macrophages in establishing an immunosuppressive PCa microenvironment, thus proposing a promising strategy for targeting YY1 in macrophages to treat advanced PCa.

RESULTS

In vivo YY1 overexpression displayed an increased M2 macrophage infiltration and PCa progression

Human YY1 is a highly conserved protein with sequences of 99.8% homology to that in mice.³² Therefore, to understand the in vivo role of YY1, we constructed a transgenic mouse model overexpressing YY1 (oe-YY1 transgenic mice; online supplemental figure 1A). First, we dissected paired oe-YY1 transgenic and wild-type mice under natural growth condition at the age of 20 weeks and found no obvious abnormal morphological differences in multiple organs, including the reproductive system, in both groups (online supplemental figure 1B). Although minimal morphological changes were observed, we speculated that in vivo YY1 overexpression might cause biochemical or immune system alterations. Therefore, we extracted peritoneal cavity–derived macrophages (PCDMs) and bone marrow–derived macrophages (BMDMs) from oe-YY1 transgenic and wild-type mice. Using flow cytometry, we found that the proportion of CD163⁺ M2, but not the CD86⁺ M1, macrophages was significantly increased in oe-YY1 mice (PCDM, 53.63 \pm 4.39% vs 40.18 \pm 2.74%, $p=0.002$; BMDM, 25.03 \pm 4.06% vs 14.10 \pm 2.63%, $p=0.004$; figure 1A–C, online supplemental figures 1C–E).

M2 macrophages are widely recognized as a tumor-promoting cell subtype; therefore, tumorigenesis experiments were conducted to identify the role of YY1 in tumor progression (online supplemental figure 1F). The mouse PCa cell line RM-1 was subcutaneously implanted on the back of mice, and we found that the subcutaneous tumors grew significantly faster in oe-YY1 transgenic mice than that in wild-type mice (figure 1D). The tumors were then harvested to test the tumor-infiltrated macrophages by immunohistochemistry (IHC) staining, and the density and proportion of CD163⁺ cells increased in oe-YY1 mouse tumors (figure 1E, online supplemental figure 1). Intriguingly, we also observed low infiltration of CD4⁺ and

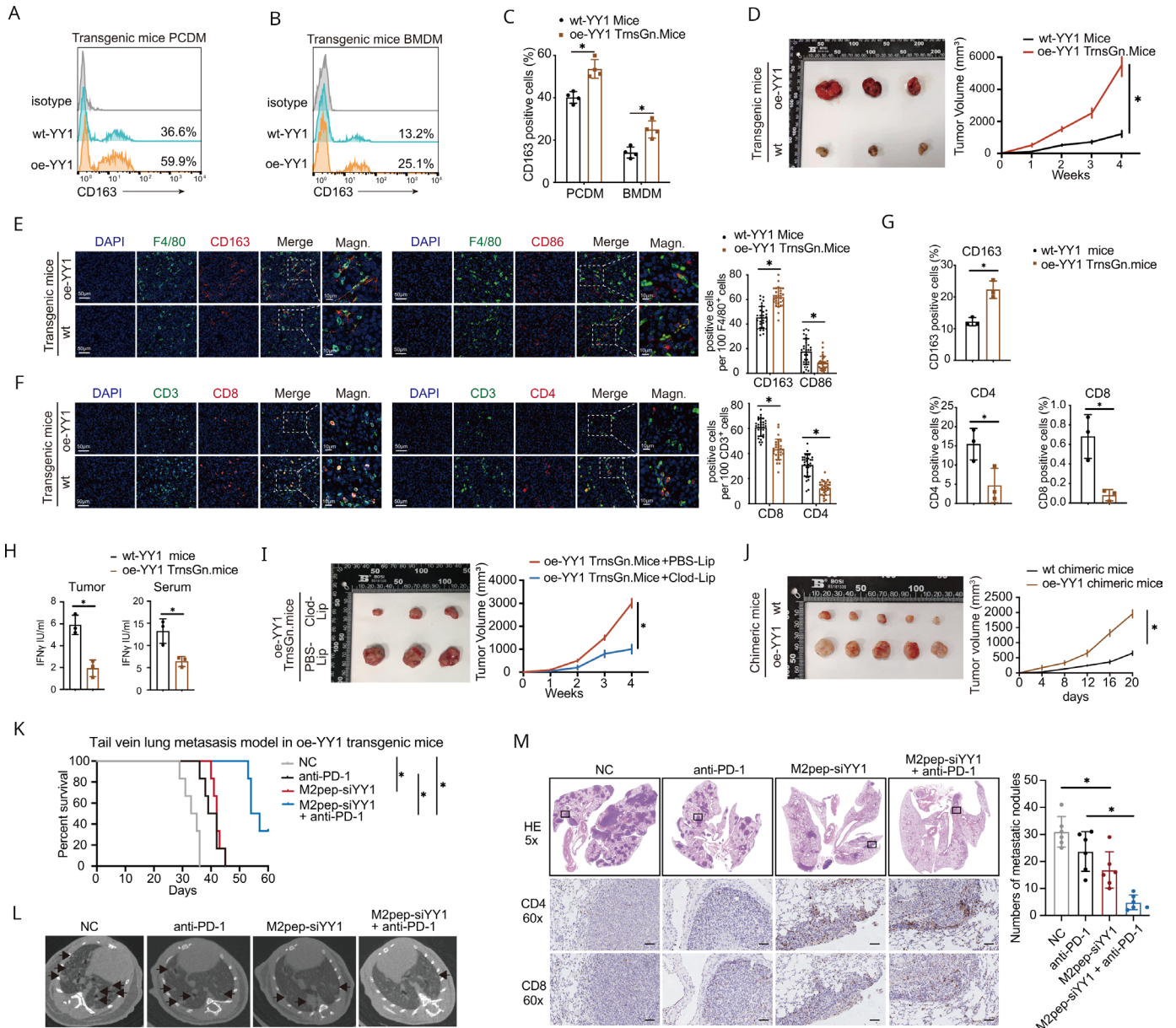


Figure 1 In vivo YY1 overexpression increased M2 macrophage infiltration and prostate cancer progression. (A–C) Flow cytometry assay of CD163 in peritoneal cavity–derived and bone marrow–derived macrophages (PCDM and BMDM) derived from transgenic mice overexpressing YY1 or wild-type mice. (D) RM-1 cells were subcutaneously injected into transgenic mice overexpressing YY1 or wild type, and tumor volume was examined during the next 4 weeks. (E, F) Multiplex fluorescence immunohistochemistry staining of the indicated subcutaneous tumor tissues showed the expression of YY1 and the infiltration of F4/80⁺CD163⁺ and F4/80⁺CD86⁺ macrophages, CD3⁺CD4⁺ and CD3⁺CD8⁺ T cells. (G) Flow cytometry of harvested subcutaneous tumors showing the CD163, CD4, and CD8 proportion in tumor-infiltrated immune cells. (H) ELISA showed the IFN γ expression in tumor tissue suspension and the indicated mice serum. (I) RM-1 cells were subcutaneously injected into oe-YY1 mice, and clodronate liposome/PBS liposome was intraperitoneally injected 7 days before subcutaneous tumorigenesis. (J) RM-1 subcutaneous tumorigenesis in oe-YY1 chimeric and wild-type mice. (K) RM-1 cells were injected into the tail vein of oe-YY1 transgenic mice aged 6–8 weeks followed by the indicated treatments to construct pulmonary metastasis model (6 mice every group), and Kaplan-Meier survival plot visualized the survival proportion of indicated groups. Premixed M2pep-siYY1 was injected by tail vein every 4 days at a dose of 15 mL/kg 2 weeks after the tumor cells were injected. Anti-PD-1 was given intraperitoneally every 4 days at a dose of 8 mg/kg 2 weeks after the tumor cells were injected. (L) CT scan of the lung was conducted 30 days after the tumor cells were injected. The black arrow points to the visible pulmonary nodules under CT scan. (M) Representative images show the H&E staining and immunohistochemistry staining of CD4 and CD8 in the indicated groups. Scale bar, 50 μ m. * p <0.05.

CD8⁺ cells in oe-YY1 mice tumors (figure 1F). To confirm these results, we performed flow cytometry on tumor tissue suspensions. The proportion of M2 macrophages

marked with CD163 from all monocytes gated by F4/80 increased in oe-YY1 mice (22.30 \pm 2.74% vs 12.22 \pm 1.29%, p =0.035, figure 1G, online supplemental figure 1H). In

addition, oe-YY1 mice also showed a decreased proportion of tumor-infiltrated CD8⁺ cytotoxic T cells ($0.08\pm 0.06\%$ vs $0.68\pm 0.22\%$, $p=0.047$) and CD4⁺ T helper cells ($4.63\pm 4.47\%$ vs $15.47\pm 4.13\%$, $p=0.017$) (figure 1G, online supplemental figure 1H). An extremely low proportion of CD8⁺ T cells was detected in all tumor tissue cells, but the IFN γ detected in mice serum (6.40 ± 1.14 IU/mL vs 13.23 ± 2.76 IU/mL, $p=0.017$) and tumor tissue suspension (1.93 ± 0.76 IU/mL vs 5.90 ± 0.89 IU/mL, $p=0.004$) was significantly lower in oe-YY1 mice than in wild-type mice (figure 1H), indicating a reduced anti-tumor activity of T lymphocytes in oe-YY1 transgenic mice. We used the lung metastatic tumor model of mice to verify the stronger PCa tumorigenesis in oe-YY1 transgenic mice (online supplemental figure 1I). Moreover, the tumorigenic effect of YY1 was suppressed when oe-YY1 mice were intraperitoneally injected with clodronate liposomes, a macrophage scavenger, 1 week before subcutaneous tumor implantation, which also verified the tumor-promoting role of macrophages (figure 1I). We also constructed chimeric mice by injecting bone marrow cells from oe-YY1 transgenic mice into wild-type mice (online supplemental figure 1A). We found that in both subcutaneous and prostate orthotopic transplanted tumor models, tumorigenesis in YY1 chimeric mice was significantly increased compared with that in the control group (figure 1J, online supplemental figure 1J).

Furthermore, the M2 macrophage-targeting peptide M2pep, described by Cieslewicz *et al.*³³ was synthesized on a liposome carrier loaded with YY1 siRNA (M2pep-siYY1) to target YY1 on M2 macrophages. M2pep-siYY1 or control siRNA was first injected into the RM-1 subcutaneous tumor in wild-type mice every 4 days for 4 weeks. We found that the size of the tumor reduced in the M2pep-siYY1 group, and the IHC of the harvested tumor showed low expression of YY1 in CD163⁺ cells (online supplemental figures 1F,K,L). Oe-YY1 transgenic mice were used to verify the role of targeting YY1 in PCa immunotherapy. We constructed a lung metastasis mouse model by tail vein injection of RM-1 cells into oe-YY1 mice. Premixed M2pep-siYY1 was administered by tail vein every 4 days at a dose of 15 mL/kg after confirming comparable pulmonary metastasis using CT scan 18 days after RM-1 cell injection. Treatment with M2pep-siYY1 showed no change in body weight, behavior, and appearance in the different groups but significantly prolonged the survival ($p<0.001$, figure 1K). Considering that macrophage YY1 could inhibit the proliferation and function of T cells in the tumor and the fact that the effect of immune checkpoint inhibitors largely depended on dysfunctional T-cell infiltration, we introduced the PD-1 inhibitor based on M2pep-siYY1 treatment. Although PD-1 blockade showed a comparable prognosis to M2pep-siYY1, the combination of both therapies significantly reduced the lung metastatic nodules observed by CT scan and prolonged the survival of the mice (figure 1K,L). Two mice in each group were sacrificed at the fifth week after tumor cell injection. H&E and IHC staining showed that the M2pep-siYY1 treatment

with PD-1 blockade significantly reduced the number of pulmonary nodules and increased the number of infiltrated CD8⁺ and CD4⁺ T cells in the tumor stroma (figure 1M, online supplemental figure 1M). In summary, we demonstrated that in vivo global overexpression of YY1 in mice resulted in increased tumor infiltration by M2 macrophages and promoted PCa progression. We also revealed the therapeutic potential of targeting M2 macrophage YY1 in PCa.

Increased YY1 in human PCa tissue correlated with a high CD163⁺ M2 macrophage content

To validate the relationship between YY1 and macrophages, we examined the expression of YY1 and CD163 in PCa and adjacent non-cancerous tissues using IHC staining in our clinical cohort. Interestingly, we found that YY1 was not only expressed on malignant cells but also showed a comparable expression level in the tumor stroma where CD163⁺ macrophages infiltrated, especially in macrophage-like cells (figure 2A, online supplemental figures 2A,B). We then performed multiplex fluorescence IHC assay of DAPI/CD163/YY1, which further validated the expression of YY1 on some subsets of tumor stroma infiltrated by CD163⁺ macrophages (figure 2B,C). To test this in a more standardized condition, we constructed tissue microarrays containing normal tissue, PCa tissue (primary PCa with Gleason grade 6–10 and castration-resistant PCa, CRPC), and metastatic lymph nodes (online supplemental figure 2C). The area of tumor stroma was marked in each tissue core, and the YY1 score of the tumor stroma was evaluated as described in Materials and methods section (figure 2D). We found that the YY1 scores in primary tumor tissues (3.7 ± 1.6) and metastatic lymph nodes (5.2 ± 1.0) were significantly higher than those in the normal control tissue (1.2 ± 1.1 , $p<0.001$, figure 2D,E), and YY1 score was also positively correlated to higher Gleason grade in primary PCa (online supplemental figure 2D). In addition, the subgroups with increasing YY1 score (YY1 score 0–2 vs 3–4 and 5–6) showed an ascending CD163 density (4.6 ± 2.4 cells/HPF vs 5.9 ± 3.5 cells/HPF vs 11.1 ± 5.0 cells/HPF) in the respective area of tumor stroma ($p<0.001$, figure 2D,F). Next, the prognostic information of the tissue microarray was also analyzed, and we found that the higher YY1 score of the tumor stroma led to a worse biochemical recurrence (BCR)-free survival of PCa ($p=0.020$, figure 2G). In addition, the difference in BCR-free survival was significant when only patients with a high density of CD163 in the YY1 high expression group were included ($p=0.004$, figure 2H, online supplemental figure 2E). In summary, by analyzing clinical prostate tissues, we found that YY1 was expressed on prostatic tumor-infiltrated M2 macrophages and that YY1 expression in the tumor stroma was also positively correlated with CD163⁺ macrophage content.

YY1 was upregulated via the IL-4/STAT6 pathway and participated in M2 macrophage polarization

Since we observed a positive correlation between YY1 and M2 macrophage markers, we conducted in vitro

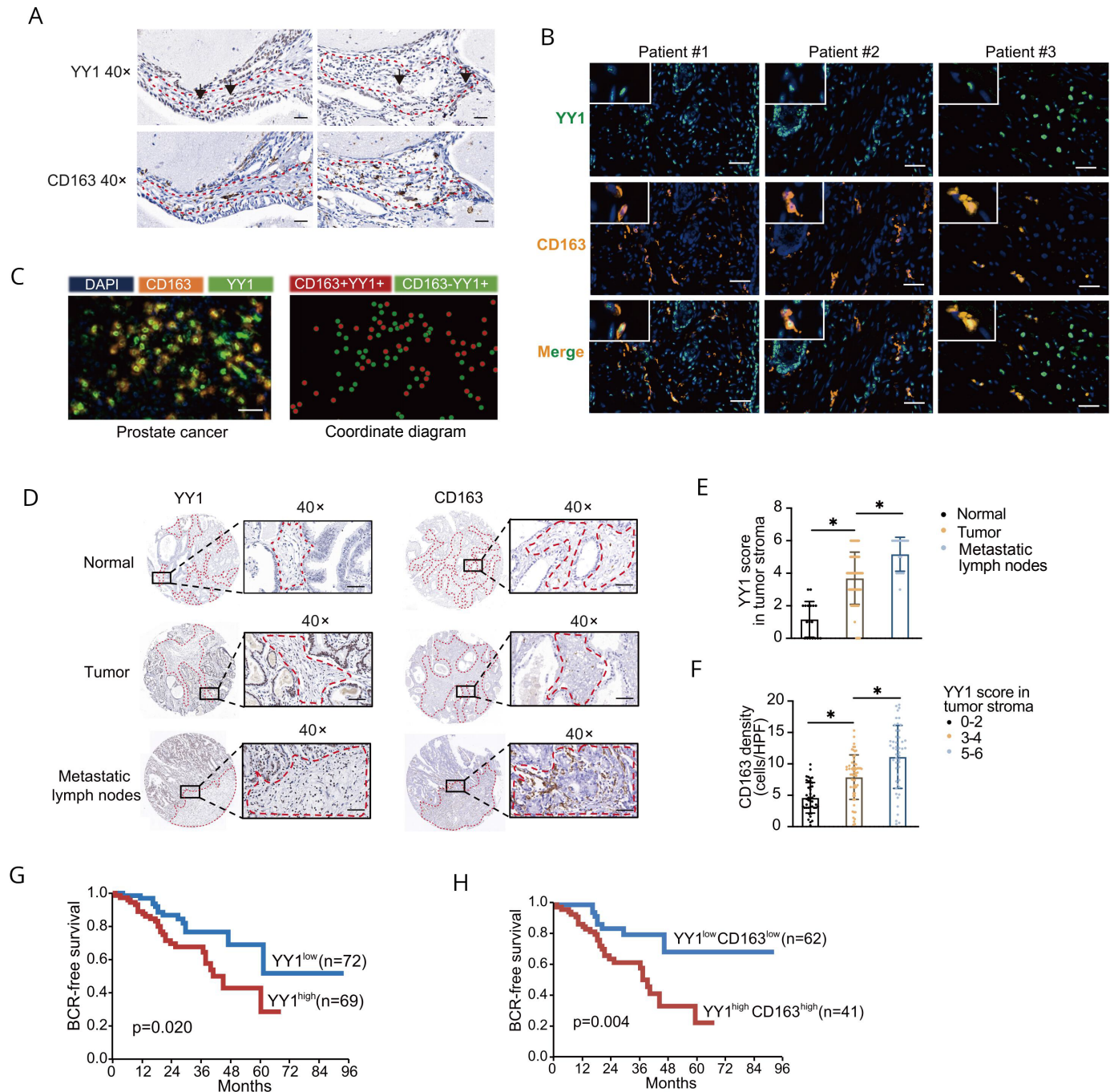


Figure 2 YY1 was positively correlated with CD163⁺ M2 macrophages in human prostate cancer. (A) Immunohistochemistry staining of YY1 and CD163 were conducted in large slices of prostate cancer tissue. Black arrow points to representative cells expressing YY1 in tumor stroma area. Scale bar, 50 μ m. (B) Representative images of three patients with multiplex fluorescence immunohistochemistry (IHC) showed a high expression of YY1 on CD163⁺ M2 macrophages in tumor stroma. (C) The left panel is the representative image of prostate cancer, in which blue is 4',6-diamidino-2-phenylindole, orange is CD163, and green is YY1. The right panel displays a corresponding diagram derived from the R script based on the coordinate of positive cells in multiplex fluorescence IHC, in which red refers to CD163 and YY1 double-positive cells and green refers to YY1 single-positive cells. Scale bar, 20 μ m. (D) Representative image of CD163 and YY1 IHC staining from tissue microarray containing a prostatic tumor, metastatic, and normal tissue. Red dashed line marks the tumor stroma area. Scale bar, 50 μ m. (E,F) YY1 score in tumor stroma and CD163 density (cells/high-power field (HPF)) in the tissue microarray of prostate cancer were evaluated by pathologists. (G,H) Higher expression of YY1 shows a worse biochemical recurrence (BCR)-free survival ($p=0.020$), while the patients with high expression of both YY1 and CD163 have significantly worse BCR-free survival ($p=0.004$). * $p<0.05$.

experiments to confirm whether YY1 participated in the M2 polarization of macrophages. After differentiating THP-1 cells into M0 macrophages (THP-1-PMA cells) in

a medium containing 100 ng/mL phorbol 12-myristate 13-acetate (PMA) for 48 hours (online supplemental figure 3A), the cells were further cultured in 20 ng/mL

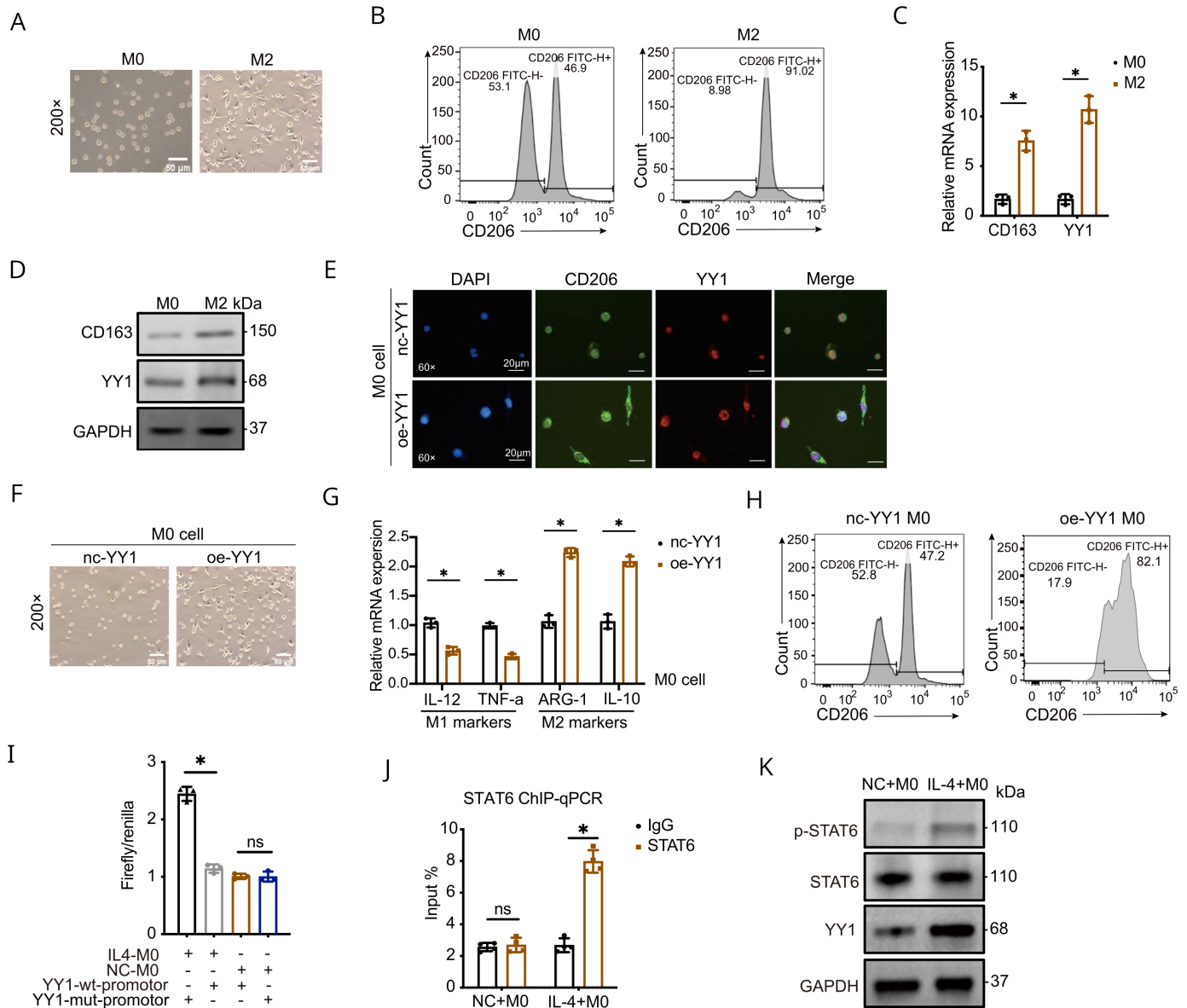


Figure 3 YY1 was upregulated by IL-4/STAT6 pathway and participated in M2 macrophage polarization. (A) Morphological changes (from suspended cells to antennal, spindle-shaped adherent cells) on the induction of M0 cells to M2 macrophages. (B) Higher proportion of CD206 in M2 macrophages (91.0% vs 9.0%) compared with M0 cells (46.9% vs 53.1%) was observed by flow cytometry. (C) Quantitative reverse transcription (qRT)-PCR analysis showed the different mRNA expressions of CD163 and YY1 in M2 or M0 cells. (D) Western blotting assay of CD163 and YY1 in M2 or M0 cells. (E) Representative multiplex fluorescence immunohistochemistry images of YY1 and CD206 colocalization in oe/nc-YY1 M2 macrophages. Scale bar, 20 μ m. (F) M2-like morphological change was displayed on YY1 overexpression in M0 macrophages. (G) mRNA expression of M1 (IL-12 and TNF- α) and M2 markers (IL-10 and ARG1) was tested by qRT-PCR in oe/nc-YY1 M0 macrophages. (H) Higher proportion of CD206 in oe-YY1 M0 cells (82.1% vs 17.9%) than in nc-YY1 (47.2% vs 52.8%) was observed by flow cytometry. (I) Luciferase assay showed that IL-4 increased the activity of YY1 promoter in M0 macrophages. (J) ChIP-qPCR showed significantly increased interaction between YY1 and STAT6 in IL-4 stimulated M0 macrophages. (K) High p-STAT6 and YY1 expression in IL-4 stimulated M0 macrophages as showed by western blotting. * $p < 0.05$.

IL-4 for another 24 hours for M2 polarization (figure 3A). Flow cytometric analysis confirmed the induction of M2 macrophages by detecting that the proportion of the M2 marker CD206 in IL-4 treated M0 macrophages was approximately two times higher than that in M0 cells ($p < 0.001$, figure 3B). M2 macrophage polarization was also verified using qRT-PCR and western blotting of CD163, and the expression of YY1 in IL-4-stimulated M0

macrophages was also significantly increased compared with M0 macrophages (figure 3C,D). Multiplex fluorescence IHC verified that YY1 was localized to M2 macrophages (online supplemental figure 3B). Thus, we successfully induced M2 macrophages in vitro and found that YY1 is highly expressed in M2 macrophages.

Interestingly, we observed morphological changes similar to those observed in M2 macrophage induction

(suspended cells to antennal, spindle-shaped adherent cells) when YY1 was overexpressed (oe-YY1) in M0 macrophages (figure 3E,F) and peripheral blood mononuclear cell (PBMC)-derived macrophages (online supplemental figure 3C), indicating that YY1 may participate in M2 macrophage polarization. To confirm our hypothesis, we examined M1/M2 macrophage markers using qRT-PCR and found that YY1 overexpression increased IL-10 and Arg1 (M2 markers) and the decreased IL-12 and TNF- α (M1 markers) expression (figure 3G). A high percentage of CD206 in oe-YY1 M0 macrophages, which were first gated with F4/80, was also observed using flow cytometry (figure 3H). These results indicated that YY1 participates in M2 macrophage polarization.

Subsequently, to clarify why YY1, both at mRNA and protein levels, was upregulated in M2 macrophages, the JASPAR database was used to predict the potential transcriptional factors (TFs) binding to the YY1 promoter. Interestingly, STAT6, a key TF in the IL-4 signaling pathway involved in M2 macrophage polarization, potentially binds to the YY1 promoter. Dual-luciferase reporter assays and chromatin immunoprecipitation (ChIP) assays were conducted to confirm the results (figure 3I,J). Moreover, a high phosphorylation level of STAT6 was observed in IL-4-stimulated M2 macrophages (figure 3K). Taken together, we confirmed that YY1 is upregulated via the IL-4/STAT6 pathway and participates in M2 macrophage polarization.

YY1 increased M2 macrophage-induced PCa malignancy

Because YY1 participated in M2 macrophage polarization, a recognized tumor-promoting subtype, we examined whether YY1 expression in macrophages affected PCa progression. First, the tumor-promoting role of M2 macrophages was verified by collecting conditioned medium (CM) from M0 and M2 macrophages to co-culture with the PCa cell lines DU145 (figure 4A, online supplemental figure 3D). Next, PCa cells were treated with the CM from YY1 overexpressed or suppressed M2 macrophages. The results showed that YY1 overexpression in M2 macrophages increased, whereas its knock-down decreased the proliferation, colony formation, and migration of PCa cells (figure 4B,F). Since M2 macrophages induce epithelial-mesenchymal transition (EMT) in cancer cells, we examined several EMT markers using qRT-PCR and western blotting. We found that the expression of vimentin and N-cadherin in DU145 cells increased by 2.49 ± 0.12 ($p < 0.001$) and 2.63 ± 0.21 times ($p < 0.001$), respectively, when treated with oe-YY1 M2 CM compared with the control-treated cells (online supplemental figures 3E,F). The oe-YY1 M2 CM-treated LNCaP cells also showed significantly decreased expression of E-cadherin and elevated expression of N-cadherin and Snail (online supplemental figures 3G,H), while no significant changes in PD-L1 expression were observed (online supplemental figure 3I). Furthermore, the organoids' average radii and area of human primary cancer cells from patients with PCa also increased when cultured for 14 days with oe-YY1

PBMC-derived macrophage's CM (figure 4G, online supplemental figure 3J).

An *in vivo* mouse model was used to validate the role of YY1 in M2 macrophage-induced tumorigenesis. RM-1 cells were mixed with oe-YY1 mouse M2 macrophages (M2 RAW264.7) or control wild-type M2 RAW264.7. Both groups of cells were subcutaneously injected into the back of C57BL/6 mice, and the tumor volume was examined every week before being sacrificed 4 weeks after tumor implantation. The tumor size and weight generated by RM-1 cells increased significantly when mixed with oe-YY1 M2 RAW264.7 cells ($p < 0.001$, figure 4H). Meanwhile, cells identical to those in the subcutaneous models were injected through the tail vein to establish a pulmonary metastasis model, and the oe-YY1 group showed significantly increased the metastatic seeding in the lungs (figure 4I). In IHC assays, the expression of CD163 was significantly upregulated in both subcutaneous and metastatic tumors with M2 RAW264.7 cells after YY1 overexpression (figure 4H,I), suggesting that YY1 expression in M2 macrophages is critical for M2 macrophage-mediated PCa progression and metastasis *in vivo*.

Next, we conducted RNA sequencing of LNCaP cells treated with oe-YY1 M2 macrophage CM or control CM. Gene Ontology analysis and gene set enrichment analysis (GSEA) indicated that upregulated genes in tumor cells treated with oe-YY1 M2 CM were enriched in the NF- κ B and JAK-STAT pathways (figure 4J,K), and western blotting assay demonstrated a high expression of p-STAT3 and p65 (figure 4I). In summary, these results suggest that YY1 in M2 macrophages positively regulates PCa malignancy by activating the NF- κ B and JAK-STAT signaling pathways.

YY1 upregulated IL-6 in macrophages to promote prostate malignancy

Since macrophages are the main source of cytokines in the TME, we investigated the cytokines regulated by YY1 in M2 macrophages. We performed liquid suspension chip assays with 27 cytokines related to tumor immunity in oe-YY1 and si-YY1 M2 macrophage CM, as well as in nc-YY1 M2 CM. IL-6 level in M2 macrophage CM were significantly upregulated (9.05 ± 0.57 times, $p < 0.001$) in the oe-YY1 group compared with the control group, while it was significantly downregulated (0.17 ± 0.05 times, $p < 0.001$) on YY1 suppression (figure 5A,B). We also confirmed that both IL-6 mRNA and protein levels were regulated by YY1 in M2 macrophages (figure 5C-E, online supplemental figure 4A). Moreover, we observed decreased expression of IL-6 on suppressing YY1 in the peripheral blood monoculture cell (PBMC)-derived macrophages (0.27 ± 0.18 vs 1.00 ± 0.11 , $p < 0.001$, online supplemental figure 4B). RNA sequencing of oe/nc-YY1 THP-1 cells indicated that genes overexpressed in oe-YY1 THP-1 cells were also enriched in the IL-6 signaling pathway (Normalized Enrichment Score=1.75, $p = 0.005$, online supplemental figure 4C).

To further identify whether IL-6 is critical for the YY1-induced tumor-promoting microenvironment of PCa, an

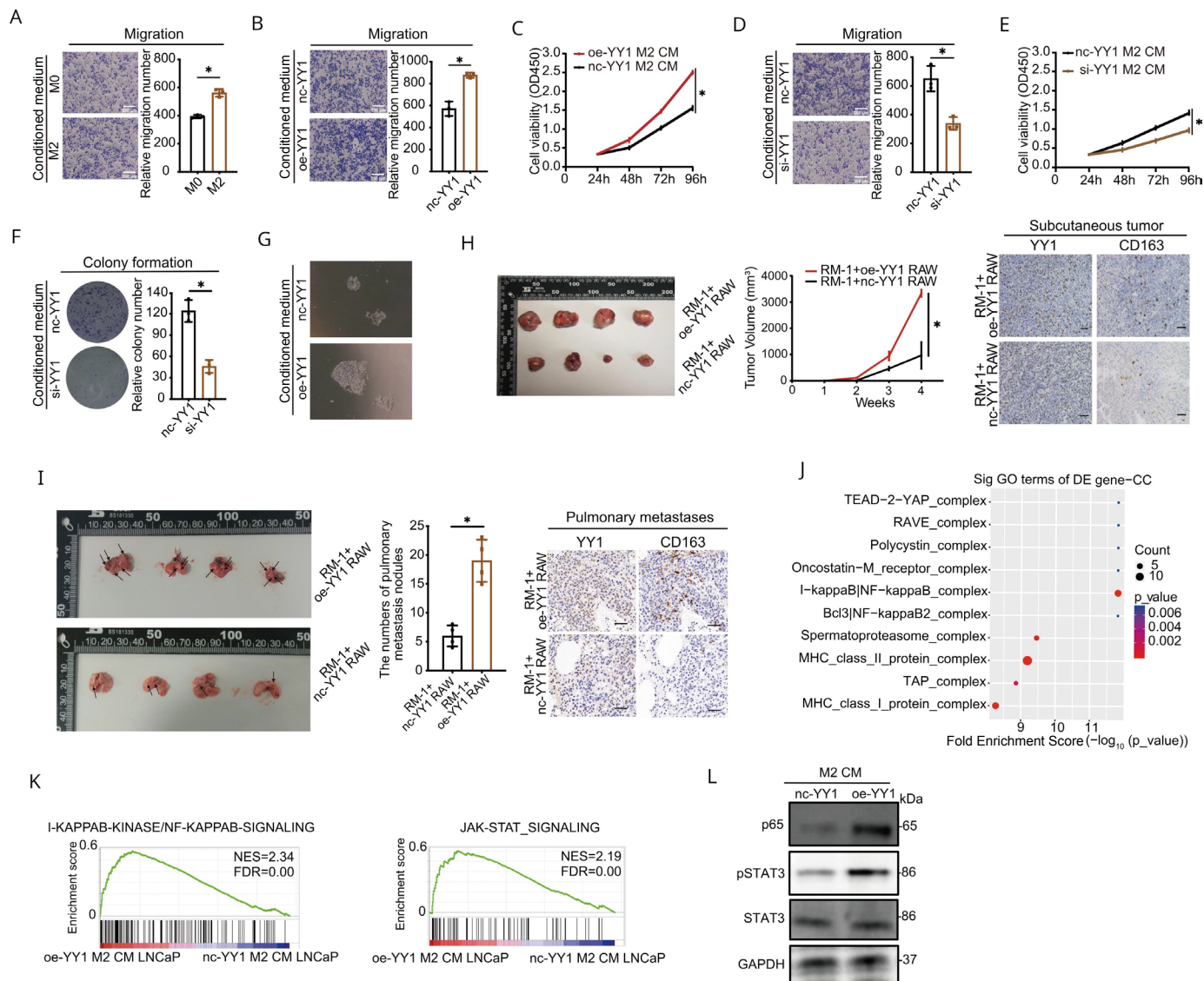


Figure 4 YY1 increased M2 macrophage-induced PCa malignancy. (A) The migration of prostate cancer cells DU145 was increased when treated with conditioned medium (CM) from M2 macrophages compared with treatment with M0 CM. (B–F) The migration (B) and proliferation (C) of DU145 cells was increased on treatment with the CM of YY1 overexpressed M2 macrophages, while there is a decrease in the migration (D), proliferation (E), and colony formation (F) of DU145 cells on treatment with the CM of YY1 knocked down M2 macrophages. (G) Primary cancer cells from patients with prostate tumor were co-cultured with CM from peripheral blood mononuclear cell (PBMC)-derived macrophages, and representative images displayed the increasing sphere formation ability in those cultured with oe-YY1 PBMC-derived macrophage CM. (H) RM-1 cells mixed with oe-YY1 M2 macrophages (M2 RAW264 cells) or control M2 RAW264 cells were subcutaneously injected into the backs of C57BL/6 mice, and tumor volume was examined during the next 4 weeks. Scale bar, 50 μ m. (I) RM-1 cells mixed with oe-YY1 M2 RAW264 cells or control M2 RAW264 cells were injected into the caudal vein of C57BL/6 mice, and pulmonary metastasis nodules were counted after 6 weeks. Arrow directed to the representative nodules. (J,K) Gene Ontology and gene set enrichment analyses displayed that the upregulated genes in LNCaP cells treated with oe-YY1 M2 macrophage CM were enriched in the NF- κ B and JAK-STAT pathway components. (L) The expression of p-STAT3 and p65 in LNCaP cells treated with oe-YY1 M2 macrophage CM was increased as shown by western blot. * $p < 0.05$.

exogenous recombinant IL-6 (rIL-6) was added to the CM from YY1-knockdown M2 macrophages to address the malignant behavior of PCa cells. After treatment with rIL-6, the malignant cells showed enhanced proliferation, colony formation, migration, and wound-healing properties, and rIL-6 treatment also rescued these properties of PCa cells attenuated by co-culture with YY1-knockdown CM (figure 5F,I). Moreover, adding the IL-6 antibody to

the CM from oe-YY1 M2 macrophages not only decreased the malignant behaviors of PCa cells (figure 5J–M) but also downregulated the expression of EMT (online supplemental figure 4D) and cancer cell stemness markers of malignant cells (online supplemental figure 4E). Taken together, YY1-mediated upregulation of IL-6 in macrophages is crucial for the protumorigenic TME in PCa.

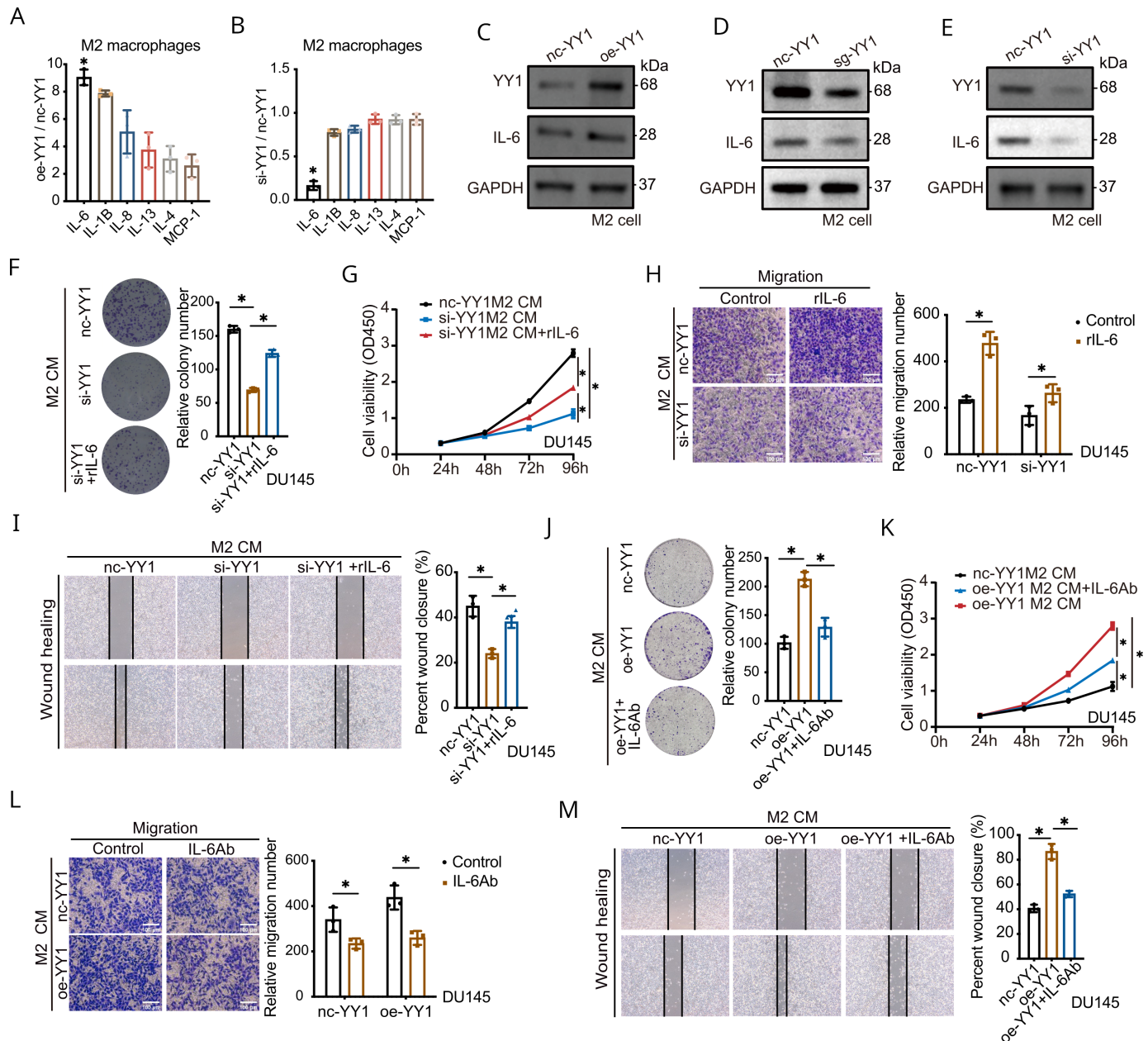


Figure 5 IL-6 upregulation by YY1 in M2 macrophages increased prostate cancer malignancy. (A,B) Cytokine microarray assay shows the highest increase of IL-6 in oe-YY1 M2 macrophage CM (A), and reduction of IL-6 in si-YY1 M2 macrophage CM (B). (C–E) qRT-PCR followed by western blotting assay showed the changes in IL-6 in oe-YY1 (C), sg-YY1 (D), and si-YY1 (E) in M2 macrophages. (F–J) Colony formation (F), proliferation (G), migration (H), and wound healing (I) of DU145 cells after adding an exogenous recombinant IL-6 (rIL-6) to si-/nc-YY1 M2 macrophage CM. (J–M) Colony formation (J), proliferation (K), migration (L), and wound healing (M) of DU145 cells after adding the IL-6 antibody to oe-/nc-YY1 M2 CM. * $p < 0.05$.

YY1 regulated IL-6 expression by modulating p300, p65, and CEBPB as a transcriptional complex

To further investigate the detailed mechanism of IL-6 regulation by YY1 in macrophages, we predicted the principal TFs in the IL-6 promoter region according to the JASPAR database. Intriguingly, four YY1 binding sites (P1–P4) were found in the IL-6 promoter region, and we also found that the motifs of YY1, CEBPB, and p65 were located near the IL-6 promoter (figure 6A). YY1 interacts with p300/p65 to promote the EMT of tumors,³⁴ and the stabilization of p300 increases the IL-6

transcription in M2 macrophages and malignant cells.³⁵ p65 is one of the most abundant members of the NF- κ B family, which is a classic upstream pathway that promotes IL-6 expression, and CEBPB is a TF that promotes the transcription of IL-6.^{36,37} Using bioinformatics analyses of the interactions between these four proteins, we found that YY1 bound to the other proteins and could be at the center of the complex (figure 6B). Further experiments were conducted to confirm this. As expected, the ChIP-qPCR results showed that YY1, CEBPB, and p65 were all bound to the IL-6 promoter region (figure 6C–E).

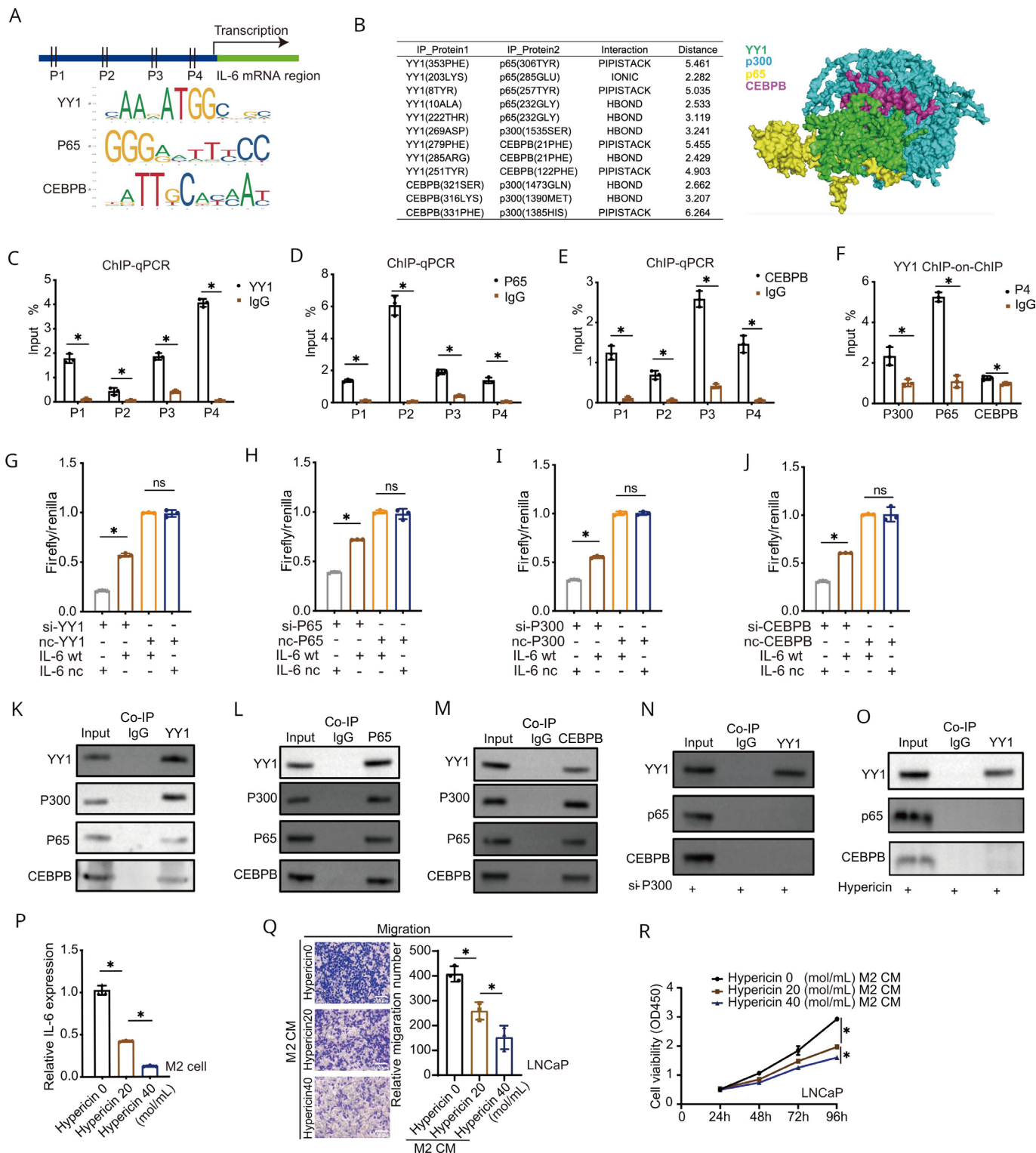


Figure 6 YY1 regulates IL-6 expression by modulating p300, p65, and CEBPB. (A) YY1, CEBPB, and p65 were predicted on the upstream of IL-6 promoter according to the JASPAR database. (B) The table and schematic show the predicted interaction between YY1 with p300, p65, and CEBPB. (C–E) Chromatin immunoprecipitation (ChIP)-qPCR showing promoter 1–promoter 4 (P1–P4), four sites in IL-6 promoter, as the binding sites of YY1 (C), p65 (D), and CEBPB (E,F). ChIP-on-ChIP analysis showed the interaction between IL-6 P1 with CEBPB, p300, and p65, respectively, in the YY1 binding protein. (G–J) Binding of YY1 (G), CEBPB (H), p300 (I), and p65 (J) to the IL-6 promoter are shown by the Luciferase assay. (K–M) Co-immunoprecipitation, followed by western blotting assay, of YY1, p65, CEBPB, and p300 shows the interaction between them. (N,O) Decrease in the immunoprecipitation between YY1, CEBPB, and p65 on the knockdown of p300 (N) and use of a YY1 complex inhibitor hypericin (O). (P) IL-6 mRNA expression was tested by qRT-PCR in M2 macrophages treated with hypericin at different doses (0, 20, 40 mol/mL). (Q,R) Migration (Q) and proliferation (R) of cultured prostate cancer cells on the treatment of the CM of M2 macrophages with different doses of hypericin (0, 20, 40 mol/mL). * $p < 0.05$.

Furthermore, ChIP-on-ChIP assays confirmed that all four proteins could bind to the P4 region of the IL-6 promoter (figure 6F). Dual luciferase reporter gene assays also confirmed that YY1, p300, p65, and CEBPB could bind to the IL-6 promoter region and enhance its promoter region activity (figure 6G–J). These results suggest that YY1, p300, p65, and CEBPB act as upstream TFs and promote IL-6 transcription by binding to the IL-6 promoter region.

Subsequently, total proteins were extracted from M2 macrophages, and co-immunoprecipitation and western blotting of YY1, p65, CEBPB, and p300 were conducted to verify the interactions (figure 6K–M). Their interactions were suppressed by p300-knockdown or the complex inhibitor, hypericin³⁸ (figure 6N,O). Moreover, hypericin reduced not only the IL-6 mRNA expression in M2 macrophages (figure 6P, online supplemental figure 4F) but also the proliferation and migration of PCa cells when mixed with M2 macrophage CM (figure 6Q,R).

YY1 promoted IL-6 transcription in macrophages by M2-specific enhancer

To validate the role of YY1 in PCa macrophages, we collected single-cell RNA sequencing data from published research in which human prostate tumor tissues were analyzed compared with normal prostate tissue.³⁹ We found that YY1 and the co-factor CEBPB both ranked among the top 20 TFs with significantly increased transcriptional activity in PCa macrophages compared with that in prostate normal tissue macrophages (figure 7A). Moreover, the IL-6/STAT3 signaling pathway was also enriched in PCa macrophages based on the single-cell RNA sequencing data (online supplemental figure 5A). These results suggest that there may be a special mechanism to enhance the regulation of IL-6 by YY1 in PCa macrophages.

The enhancer can act on the promoter region at long distances to promote the target gene transcription, and its effect is usually tissue-specific. Weintraub *et al* reported that YY1 acts as a structural regulator in the enhancer–promoter loops,³¹ and p300 in the YY1 transcription complex is a crucial marker for transcriptional enhancers.^{34–43} However, the role of YY1 in macrophage enhancers has not yet been reported. Here, we performed H3K27ac and YY1 chromatin immunoprecipitation sequencing (ChIP-seq) in M2 macrophages and THP-1 cells. Although the H3K27ac ($r=0.92$, $p<0.001$) and YY1 ($r=0.85$, $p<0.001$) signals showed an overall positive correlation between THP-1 cells and M2 macrophages (online supplemental figures 5B–C), we still identified thousands of gained or lost enhancers that changed during M2 polarization (figure 7B). In total, 15,241 enhancers were identified as M2-specific enhancers during M2 polarization. H3K27ac signals of M2-specific enhancers were quite low in THP-1 cells, and YY1 ChIP-seq signals were also enriched in M2-specific enhancers in M2 macrophages (figure 7C). Nevertheless, the YY1 ChIP-seq signals of M2-specific enhancers were

significantly decreased in THP-1 cells, suggesting a critical role of YY1 in M2 macrophages.

To identify the differential enhancers of IL-6, we used Hi-C data to identify enhancer–promoter interactions. We found an M2-specific IL-6 enhancer (chr7, 22755717–23522992) directly interacting with IL-6 promoters (figure 7B,D) and significantly stronger H3K27ac and YY1 ChIP-seq signals around this enhancer in polarized M2 macrophages than in the THP-1 cells (figure 7C). Meanwhile, BRD4, an important chromatin-binding protein for enhancer organization and gene regulation,^{44–46} was also enriched in a related enhancer fragment (online supplemental figure 5D).

To confirm the role of the IL-6 enhancer located in the Hi-C data, we constructed a luciferase gene plasmid containing an enhancer fragment with four segments (regions E1–4) (figure 7E). The cells were then co-transfected with a vector overexpressing YY1 into M2 macrophages, followed by luciferase signal measurement. Region E1 (the distal end of the enhancer fragment) was identified as the binding site of YY1 using luciferase assay and chromosome conformation capture (3C) experiments (figure 7F–G). We knocked out region E1 (sg-E1) in M2 macrophages using CRISPR-Cas9, and ELISA and qRT-PCR revealed decreased IL-6 expression (figure 7H–I). The bromodomain inhibitor, JQ1, which inhibits enhancer signaling, also downregulated IL-6 expression (figure 7J). These results indicated that the M2-specific IL-6 enhancer is important for IL-6 transcription.

Next, we conducted *in vitro* and *in vivo* experiments to verify the effect of the M2-specific enhancer on M2 macrophage polarization and function. First, JQ1-treated macrophages showed low mRNA expression of ARG-1 and IL-10, indicating suppression of M2 polarization by JQ1 (figure 7K). Moreover, when JQ1 was added to the co-culture system of DU145 cells and M2 macrophages, the migration and invasion abilities of malignant cells were significantly suppressed compared with those of the negative control (figure 7L, online supplemental figure 5E). To precisely examine the influence of the M2-specific enhancer on M2 macrophage function, sg-E1 M2 CM was used to culture DU145 cells. The malignant behavior of PCa cells decreased in the sg-E1 group (figure 7M, online supplemental figure 5F). In further *in vivo* experiments, 2 weeks after subcutaneous tumor implantation in mice, we intraperitoneally injected JQ1 (50 mg/kg/days) and CPI-637 (10 mg/kg/days), which are enhancer inhibitors targeting BRD4 and p300/CBP bromodomain, respectively, continuously for 3 weeks before the tumor was harvested and found that the tumor volume was significantly reduced compared with that of the negative control ($493\pm 62\text{ mm}^3$ vs $471\pm 45\text{ mm}^3$ vs $2230\pm 213\text{ mm}^3$, $p<0.001$, figure 7N). In conclusion, the YY1 complex upregulates IL-6 through an M2-specific enhancer, thus promoting PCa progression.

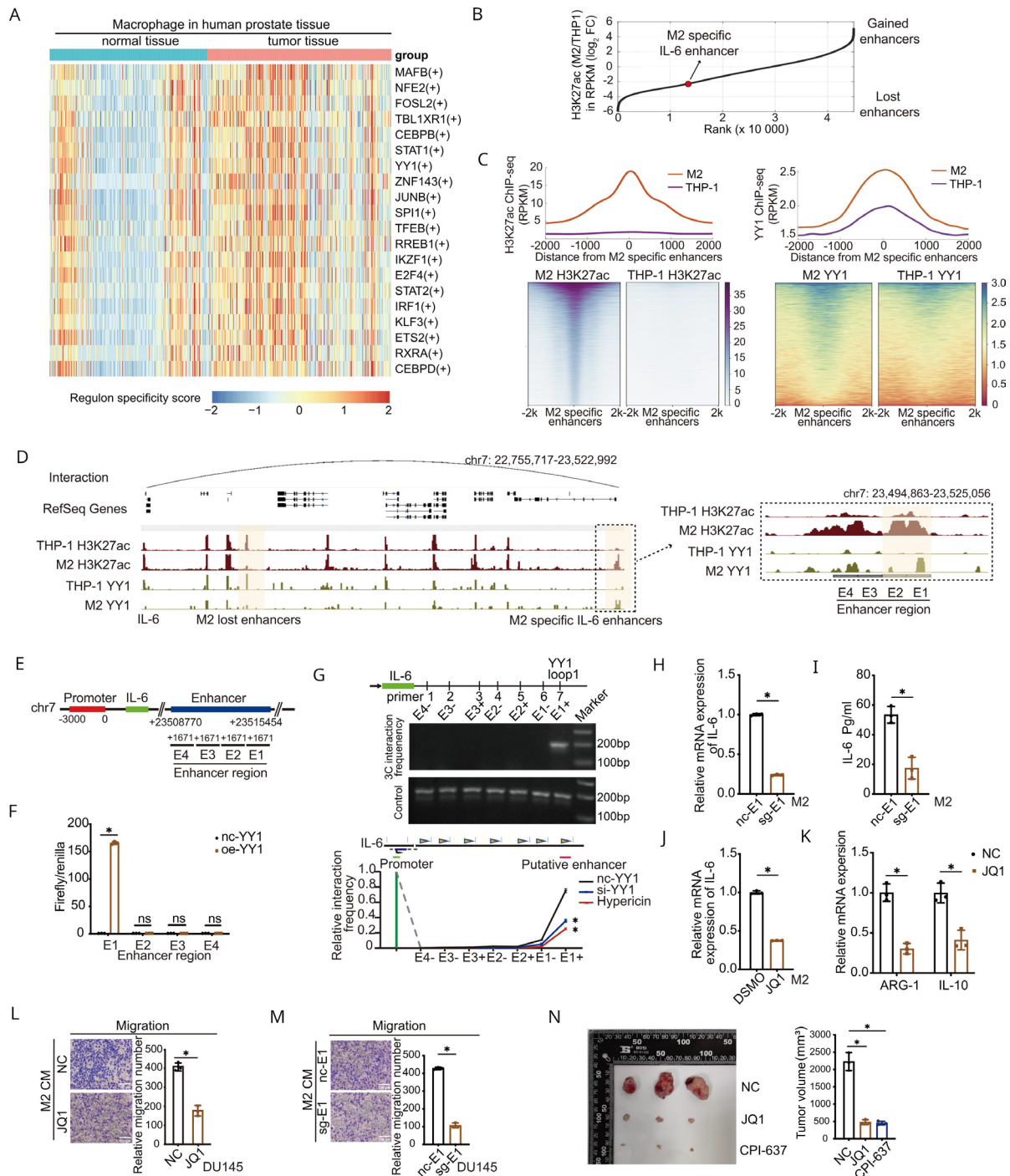


Figure 7 YY1 promotes IL-6 transcription by M2-specific enhancer. (A) Based on the single-cell RNA sequencing data set, regulons were ranked by difference of the regulon specificity score between tumor and normal prostate tissue from high to low, and the top 20 different regulons were used to plot the heatmap. (B) An M2-specific IL-6 enhancer was located by comparing H3K27ac ChIP-seq data for THP-1 cells and M2 macrophages. (C) Distribution of H3K27ac and YY1 ChIP-seq signals around M2-specific enhancers in M2 macrophage and THP-1 cells. Top panel: normalized ChIP-seq signals around M2-specific enhancers. Bottom panel: heatmap of ChIP-seq signals; each row represents an M2-specific enhancer. All rows are sorted according to the signal values. (D) IL-6 enhancer location and its interaction with IL-6 promoter as displayed by the Integrative Genomics Viewer. (E) Plasmids containing four segments (regions E1–4) of the identified enhancer. (F,G) Binding of region E1 with YY1 as shown by the luciferase assay (F) and chromosome conformation capture experiment (G) after the co-transfection of vector *oe-YY1* or *nc-YY1* into 293 T cells. (H,I) qRT-PCR assay (H) and ELISA analysis (I) showed a significant decrease in the expression of IL-6 on CRISPR/Cas9 knocking out region E1 (*sg-E1*) compared with the negative control group. (J,K) The enhancer signaling inhibitor JQ1 decreases IL-6 expression (J) and M2 markers (K) tested by the qRT-PCR assay. (L,M) The migration of DU145 cells were tested on treatment with JQ1/*nc* (L) and *sg-E1*/*sg-nc* M2 macrophage CM (M,N). JQ1, CPI-637, and blank control medium were intraperitoneally injected for 18 days into mice with subcutaneous tumors, and tumor volume was measured after 3 weeks. **p*<0.05.

YY1 formed LLPS during M2 macrophage polarization

When immunofluorescence of YY1 was conducted, the number of droplets in nuclei significantly increased in IL-4-stimulated M2 macrophages compared with that in PMA-THP-1 M0 cells (11.3 ± 3.6 droplets/cell vs 6.7 ± 3.0 droplets/cell, $p < 0.001$, [figure 8A](#)), indicating that YY1 might form condensates by LLPS. Next, we predicted the large IDRs of YY1 based on the PONDR score ([figure 8B](#)). Different concentrations of recombinant YY1-IDR-EGFP protein were mixed with 30% polyethylene glycol (PEG), whose concentration was previously confirmed using the gradient test (online supplemental figure 5G). Using fluorescence microscopy, we observed that the density of the LLPS droplets increased with the concentration of YY1-IDR-EGFP protein ([figure 8C](#)) but decreased after treatment with 1,6-hexanediol (1,6-Hex), which destroys the weak hydrophobic bonds in the medium. No droplets were detected in YY1-non-IDR-EGFP cells ([figure 8C](#)).

Next, we transfected YY1-IDR-EGFP, YY1-non-IDR-EGFP, and EGFP-labeled YY1 full-length plasmids into M2 macrophages and observed the live cells under a confocal fluorescence microscope. YY1 aggregated as punctiform droplets on the uniformly distributed background expression on cells, and the number of droplets significantly increased in the YY1-EGFP and YY1-IDR-EGFP groups compared with that in the YY1-non-IDR-EGFP group (11.4 ± 5.0 droplets/cell vs 11.7 ± 5.4 droplets/cell vs 0.9 ± 1.3 droplets/cell, $p < 0.001$, [figure 8D](#)). In addition, we observed fusion and fission in some droplets ([figure 8E](#)), and the fluorescence intensity of the nuclear punctum could be restored after photobleaching of the targeted focus ([figure 8F](#)), indicating that the nuclear condensates in macrophages were formed by LLPS. To further clarify the location of YY1 droplets in macrophages and the role of the IDR region in droplet formation, we stained DAPI after cell fixation and knocked out the YY1-IDR region by full-length YY1 CRISPR/Cas9 knockout and the non-IDR region overexpression in M2 macrophages (sg-YY1-IDR, online supplemental figure 5H). We found that YY1 droplets were mostly located in the M2 macrophage nucleus, and the number of droplets decreased significantly after YY1-IDR knockout (10.7 ± 4.2 droplets/cell vs 3.0 ± 2.0 droplets/cell, $p < 0.001$, [figure 8G,H](#)).

In addition, the predicted binding sites of YY1 in the YY1/p300/p65/CEBPB complex were located on the YY1-IDR segment ([figure 6B](#)). The immunoprecipitation assay with the EGFP antibody followed by western blotting demonstrated the interaction of p65, p300, and CEBPB with YY1-IDR-EGFP in M2 macrophages ([figure 8I](#)). We also observed the colocalization of the LLPS condensates of YY1 with p300, p65, and CEBPB ([figure 8J](#)). Meanwhile, YY1 condensates were defused by siRNA suppressing p300, p65, and CEBPB expression, as well as under the intervention of the p300/p65 complex inhibitor hypericin, in M2 macrophages ([figure 8K](#)). In brief, these results demonstrate the key role of the YY1-IDR segment in YY1 LLPS, and that the YY1/p300/p65/CEBPB complex promoted the formation of YY1-mediated LLPS in M2 macrophages.

Furthermore, when pretreated with 1,6-Hex or transfected with sg-YY1-IDR, the relative expression of M2 markers (ARG-1 and IL-10) and IL-6 in IL-4-stimulated macrophages was significantly reduced compared with the negative control ($p < 0.001$, [figure 8L,M](#), online supplemental figure 5H). In addition, the knockdown of the cofactors in the YY1 complex also decreased ARG-1 and IL-10 expression ([figure 8N](#)). In summary, we showed that the YY1 complex formed LLPS during M2 polarization and that YY1-mediated LLPS upregulated IL-6 expression in M2 macrophages.

MATERIALS AND METHODS

Tissue samples, tissue microarrays, and immunohistochemical staining

Formalin-fixed paraffin-embedded PCa tissue samples were obtained from patients who underwent radical prostatectomy at the Affiliated Zhongda Hospital of Southeast University between April 2018 and April 2021. The pathological diagnosis was confirmed by at least two pathologists. Samples from patients with non-distant metastatic PCa who did not receive ADT were included in the study. Tissue microarrays containing 141 PCa and 18 normal prostatic tissues were constructed with punches measuring 0.6 mm in diameter from blocks, including the tumor center, normal tissues adjacent to the tumor, and lymph node metastases.

For IHC, xylene and serially diluted ethanol were used for the dewaxing and dehydration of paraffin-embedded tissue sections. Tissue sections were incubated in an autoclave for 5 min at 121°C for antigen retrieval prior to incubation with primary antibodies, including YY1 (Abcam, Cambridge, UK), CD163 (Abcam), CD206 (Proteintech, Rosemont, IL, USA), CD4 (Abcam), and CD8 (Abcam), at 4°C overnight and bound antibody (Proteintech) at 37°C for 30 min. Bound antibodies were detected using the a 3,3'-diaminobenzidine kit and hematoxylin. After fixing and mounting the tissue section, the YY1 staining intensity was evaluated as follows: score A—no staining as 0, weak as 1, moderate as 2, and 3 for strong staining; score B—1 if less than 10% of stroma cells were stained, 11–50% as 2, and more than 50% as 3. The YY1 protein expression score was recorded as the sum of both scores (scores A and B). The tissue core was recognized as positively stained if the final score was >4 . The immune cells density, including markers of CD163, CD4, and CD8 markers, was measured within five random views of high-power field (HPF) each core, and the average number of CD163-positive cells/HPF was counted manually by pathologists.

Cell lines and culture

Human (LNCaP and DU145) and mouse (RM-1) PCa cell lines were purchased from the American Type Culture Collection (ATCC, USA). Human monocyte THP-1 and mouse macrophage RAW264.7 cell lines were purchased from the Shanghai Institutes for Biological Sciences. Cells

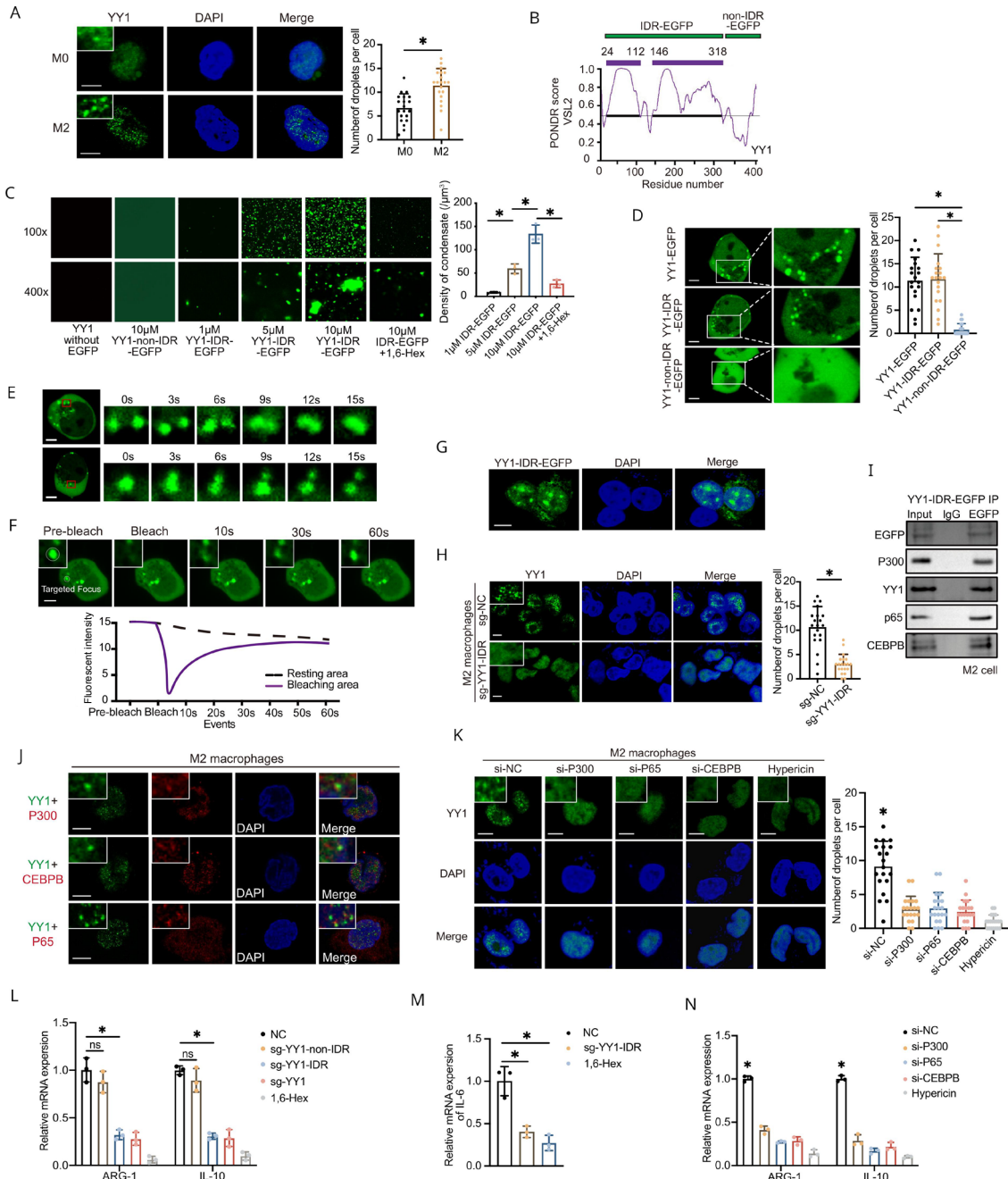


Figure 8 YY1 formed liquid-liquid phase separation during M2 macrophage polarization. (A) Immunofluorescence assay using confocal fluorescence microscopy showed patterns of YY1 droplets distribution in M0 (PMA-THP-1 cells) and M2 macrophages (IL-4 stimulated PMA-THP-1 cells). Scale bar, 5 μ m. (B) POND VSL2 score of YY1 displayed according to the database of pondr.com, with the purple bar showing the sites of intrinsically disordered regions (IDRs) and the green bar showing segments of IDR-EGFP and non-IDR-EGFP. (C) Representative images of phase separation droplets based on IDR-EGFP with different protein concentrations or with 1,6-hexanediol (1,6-Hex). Two panels on the left show the images when either YY1 or non-IDR-EGFP alone was added. (D) Live M2 macrophages transfected with YY1-IDR-EGFP, YY1-EGFP, and YY1-non-IDR-EGFP were observed under confocal fluorescence microscope. Scale bar, 2 μ m. (E) The process of fusion and fission in the YY1-IDR-EGFP mediated droplets. (F) Fluorescence intensity of the condensate during fluorescence recovery after photobleaching assay. The white circle in the top left panel shows the photobleaching targeted focus range where it is bleached for 1 s. Scale bar, 2 μ m. (G) YY1-IDR-EGFP was displayed to localize on the M2 macrophage nuclear when the cells were fixed and stained with 4',6-diamidino-2-phenylindole (DAPI). Scale bar, 5 μ m. (H) The numbers of droplets per cell were detected in the M2 macrophages knocking out YY1-IDR (sg-YY1-IDR) or negative control (sg-NC). Scale bar, 5 μ m. (I) Immunoprecipitation with the EGFP antibody followed by western blot in YY1-IDR-EGFP transfected M2 macrophages. (J) Colocalization of YY1 droplets with p300, p65, and CEBPB in M2 macrophages. Scale bar, 5 μ m. (K) Liquid-liquid phase separation droplets of YY1 were inhibited by using siRNA to reduce p300, p65, and CEBPB expression or inhibitor of YY1 complex in M2 macrophages, respectively. Scale bar, 5 μ m. (L-N) The mRNA expression of M2 markers (IL-10 and ARG1) and IL-6 was tested by qRT-PCR in the indicated groups. * p <0.05.

were cultured in an RPMI 1640 medium (Gibco, Thermo Fisher Scientific, Waltham, MA, USA) containing 10% fetal bovine serum (FBS; Gibco), 1% penicillin G, and streptomycin sodium (Gibco) in 95% humidified air at 37°C and 5% CO₂. THP-1 cells were differentiated into M0 macrophages by incubation with 100 ng/mL phorbol 12-myristate 13-acetate (PMA; Sigma-Aldrich, St. Louis, MO, USA) for 48 hours. We used 20 ng/mL of IL-4 and IL-10 to polarize M0 into M2 macrophages.

For organoid culture, tumor species were sectioned into small chunks and digested using collagenase I (Gibco Life Technology, USA) and TrypLE express (Gibco Life Technology, USA) at a ratio of 1:2 in a 15 mL conical centrifuge tube (Corning, USA). Samples were incubated for 30–90 min, depending on the amount of tissue, until most of the cell clusters were suspended. The cells were then cultured for 14 days in oe-/nc-YY1 M2 condition medium and Dulbecco's modified Eagle's medium (DMEM; Gibco Life Technology, USA), containing the following growth factors: 5–50 ng/mL EGF (X-Bio Technology, China), 500 ng/mL recombinant R-spondin1 (X-Bio Technology), 100 ng/mL recombinant Noggin (X-Bio Technology), and 200 nM TGF-β/Alk inhibitor A83-01 (X-Bio Technology).

For BMDM culture, the mice were sacrificed after anesthesia, and the leg bones were kept under sterile conditions. The bone marrow was blown out using a premixed medium (RPMI1640/DMEM high glucose medium+10% FBS), and the cells were filtered through a 70 μm cell filter. A lysis buffer of erythrocytes was added into the filtered cells. The cells were then resuspended in a premixed medium (RPMI1640/DMEM high glucose+10% FBS+20 ng/mL M-CSF). IL-4 was added to the medium on the fifth day and induced for 48 hours before subsequent flow cytometry experiments. For PCDMs, 6 mL DMEM was injected into the abdominal cavity after the mice were sacrificed, and the abdomen was gently massaged for 10 min. Then, abdominal fluid was obtained using a syringe, and the abdominal cavity was rinsed twice with 5 mL phosphate-buffered saline (PBS). After centrifugation, the cells were resuspended and plated in DMEM. Cells were incubated for another 2 hours, the suspended cells were washed out, and the adherent cells were used for flow cytometry analysis.

Small interfering RNA and overexpression lentivirus

Small interfering RNAs (siRNAs) targeting YY1, p300, p65, and CEBPB were designed and synthesized by GenePharma Co. (Shanghai, China). YY1 overexpressed lentivirus (oe-YY1) was synthesized and subcloned into the GV492 plasmid (GeneChem, Shanghai, China), and an empty plasmid was used as the negative control. The plasmid maps are shown in online supplemental figures 6A–E and the siRNAs sequences are listed in online supplemental table 1. THP-1 cells were differentiated into M0 macrophages by incubation with PMA, and the oe/si-YY1 or the negative control were transfected using a transfection reagent (Vazyme Biotech, Nanjing, China)

following the manufacturer's protocol. IL-4 was used to stimulate M2 macrophages.

CRISPR-Cas9 knockout of the differential enhancer and YY1

CRISPR/Cas9 gene knockout system was constructed and validated using GeneChem. Detailed information on the synthesized oligonucleotides, including sg-YY1 and sg-enhancer 1 (sg-E1), is listed in online supplemental table 1 (YY1 gDNA-F: TTGATAAGGGGCTGGT and gDNA-R: CCACGAGAAGTACCCACCA; enhancer-1 gDNA-F: ACATTTCTCTATCGATAGGTACC and gDNA-R: CTCGAGATCTGCGATCTAAGTAAGCTTGGCAT). The GV393 plasmid map is listed in online supplemental figure 6D. CRISPR/Cas9 lentiviruses were transferred into M2 macrophages and THP-1 cells, and green fluorescent protein (GFP⁺) cells were observed under a fluorescent microscope to confirm the success of transfection.

RNA extraction and RT-PCR

RNA was extracted using an RNA extraction kit (Takara Kusatsu, Shiga, Japan) according to the manufacturer's protocol, and purified RNA was used to synthesize cDNA by reverse transcription PCR (RT-PCR) using a Hiscript II First-Strand cDNA Synthesis Kit (Vazyme Biotech). Quantitative real-time PCR was performed using the MonAmp SYBR Green qPCR Mix (Monad Biotech, Zhuhai, China). Primer sequences are listed in online supplemental table 1. Relative gene expression levels were normalized to the internal control GAPDH.

Flow cytometry

To detect cell surface markers, purified cells were stained with CD8α (553 030, BD Bioscience, NJ, USA), CD3 (555 275, BD Bioscience), CD4 (100 527, Biolegend, San Diego, CA, USA), CD163 (156 704, Biolegend), CD86 (ab77276, Abcam), and F4/80 (123110, Biolegend) and incubated at 4°C for 30 min at the recommended concentrations. For CD206 (321104; Biolegend) staining, cells were first fixed and permeabilized with the FIX & PERM Kit (MultiSciences Biotech, Hangzhou, China). Macrophages were gated using F4/80 before CD206, CD163, or CD86 proportion detection. A FACS flow cytometer (BD Biosciences, USA) was used for the flow cytometry analysis. Dead cells were excluded by using the flexible viability dye eFluor506. Isotype controls and single-stained cells were used to set the gate of positive cells for each dye.

Western blotting

Total protein was extracted using the RIPA lysis buffer (1:1000) (KeyGene Biotech, Nanjing, China), and the supernatant was collected. Protein quantification was performed using the bicinchoninic acid assay (KeyGene Biotech). The extracted total protein was separated into a 10% sodium dodecyl sulfate-polyacrylamide (SDS) gel electrophoresis and transferred onto a polyvinylidene difluoride membrane (Merck Millipore, Burlington, MA, USA). The membrane was then blocked for 1 hour in Tris-buffered saline with Tween 20 containing 5%

non-fat milk. Next, we incubated the membrane with the following primary antibodies overnight at 4°C: YY1 (1/2000, 68 kDa; Abcam), CD163 (1/2000, 150 kDa; Abcam), P300 (1/2000, 300 kDa; Abcam), IL-6 (1/2000, 20 kDa; Proteintech, Rosemont, IL, USA), P65 (1/2000, 65 kDa; Proteintech), and CEBPB (1/3000, 45 kDa; Proteintech). GAPDH (1/3000, 37 kDa; Proteintech) was used as an internal control.

Luciferase assays

The IL-6 luciferase plasmid GV238 was cotransfected with si-YY1, si-CEBPB, si-p300, si-p65, or si-NC (GeneChem) into the cells using a transfection reagent (Vazyme Biotech). The enhancer luciferase plasmid of GV238 was cotransfected with oe/nc-YY1 (GeneChem). The sequences used are listed in online supplemental table 1. A dual-luciferase reporter assay system (Promega, Madison, WI, USA) was used to measure the firefly luciferase signal followed by transfection for 48 hours. All measurements were conducted according to Promega's protocol, and the Renilla luciferase signal was used for normalization.

Liquid suspension ChIP and ELISA

The Bio-Plex Pro Human Cytokine Grp I Panel 27-plex (Wayen Biotechnologies, Shanghai, China) was used to perform the liquid suspension ChIP assay according to the manufacturer's instructions. Macrophages with oe-YY1, si-YY1, or the control were incubated with microbeads for 30 min, followed by antibody incubation for another 30 min. The Bio-Plex MAGPIX System (Bio-Rad, Hercules, CA, USA) was used to read the values after staining with streptavidin-PE.

The IL-6 ELISA Kit (Invitrogen, Thermo Fisher Scientific) was used to measure the secreted IL-6 levels in the supernatant of M2 macrophages following the manufacturer's protocol. For IFN γ detection, the peripheral blood of mice was collected 4 weeks after tumor implantation and centrifuged to obtain serum. An equal volume of tumor tissue (0.5 g) was thoroughly ground and filtered into a 10 mL tissue suspension before ELISA analysis. The IFN γ mouse ELISA Kit (Invitrogen, Thermo Fisher Scientific) was then used to detect the secreted IFN γ in the serum and tumor tissue suspension following the manufacturer's protocol.

RNA sequencing and gene set enrichment analysis

RNA was extracted from oe-YY1/nc-YY1 THP-1 or LNCaP cells treated with oe-YY1/nc-YY1 M2 macrophage CM before RNA sequencing (RNA-seq) by KangChen Biotech (Shanghai, China). GSEA was performed to study the change in the functional signaling pathways, with all annotation files downloaded from the Molecular Signatures Database (MsigDB, <https://www.gsea-msigdb.org/gsea/msigdb/>).

Wound-healing assay

Cells were inoculated into 6-well plates and treated with oe-/si-YY1 M2 macrophage CM or recombinant IL-6/

anti-IL-6. A straight scratch was made on the plate using a sterilized needle tip at a cell density of approximately 70%. The cell wound edge was marked and photographed at the starting time point under a microscope. After 12 hours, we measured the cell migration distance and analyzed the wound closure percentage.

Cell proliferation analysis

Colony formation and cell counting kit-8 (CCK-8) cell proliferation assays were performed to compare cell proliferation under different conditions. Pretreated cells were seeded in 6-well plates at 1000 cells/well density. For the colony formation assay, cells were fixed with 4% methanol for 20 min after incubation at 37°C for 2 weeks. We stained the cells using a 0.1% crystal violet dye solution and then manually counted the colonies under a light microscope. For the cell proliferation assay, CCK-8 solution from the kit (KeyGene Biotech) was added every 24 hours. The cell proliferation plots were drawn according to the optical density value measured with an automatic microplate reader.

Transwell assay

We conducted a transwell assay to test cell invasion and migration by using chemotactic chambers with and without pre-paved Matrigel (BD Pharmingen Inc., San Diego, CA, USA), respectively. The upper chamber was covered with a serum-free medium, and the lower chamber had an RPMI-1640 medium containing 10% FBS (Gibco). The upper chamber was removed after incubation for 12 hours. The migrated cells in the lower chamber were fixed with methanol, stained with crystal violet, and counted under the microscope.

Mice tumorigenicity assay

C57BL/6 male mice, aged 4–6 weeks, were purchased from the Comparative Medical Center of Yangzhou University and raised under the standard conditions at the Animal Center of Southeast University. Mice were acclimated in a laboratory environment for 2–3 weeks until 6–8 weeks of age prior to the experiments. The use of laboratory mice was approved by the Ethics Committee of the Affiliated Zhongda Hospital of Southeast University. RM-1 (5×10^6) cells transfected with oe/nc-YY1 lentivirus were injected through the tail vein or subcutaneously on the back of mice. Tumor volume was then evaluated every 4 days after injection, following the formula of $\text{length} \times \text{width}^2 / 2$. Two weeks after subcutaneous RM-1 implantation, JQ1 (50 mg/kg/day) and CPI-637 (10 mg/kg/day) were injected intraperitoneally every day for 3 weeks until the tumor was harvested.

Transgenic mice overexpressing YY1 and in vivo YY1-targeted knockdown

Transgenic mice overexpressing YY1 were constructed using PiggyBac transposon technology (Alingfei Biotechnology Co., Ltd., Jiangsu, China). The YY1 cDNA sequence was initially inserted into the pCAG promoter, followed by insertion into two inverted terminal repeat

(ITR) elements of the PiggyBac transposon system to form the ITR-pCAG-YY1-ITR transgenic vector. Transposase cRNA were co-injected with the constructed transgenic vector into the zygotes of mice by microinjection. The injected fertilized eggs were subsequently transplanted into embryos to construct founder mice. Founder mice were identified and screened using quantitative RT-PCR. A schematic diagram of the vector, YY1 gene, and transgenic DNA sequence is listed in online supplemental material.

Oe-YY1 chimeric mice were generated using the bone marrow cells from oe-YY1 transgenic mice. We injected clodronate liposomes (Clod-Lip, 10 μ L/g) into C57BL/6 mice 6 days before they were exposed to X-ray (9 cy, 8 min). We injected bone marrow cells obtained from the thighbone of oe-YY1 transgenic mice or wild-type mice (16 weeks) into these irradiated mice through the tail vein 24 hours after the exposure. Subcutaneous and lung metastatic tumor implantation was performed as described in the C57BL/6 mouse tumorigenicity assay. Clod-Lip/PBS liposomes (PBS-Lip) were administered intraperitoneally at 10 mg/kg 7 days before subcutaneous tumorigenesis. A polypeptide named M2pep, described by Cieslewicz *et al.*,³³ was synthesized by RuixiBio (Xi'an, China). M2pep was modified on a liposome carrier and loaded with YY1 siRNA (M2pep-siYY1). M2pep-siYY1 was used to treat YY1 in oe-YY1 transgenic mice following the manufacturer's protocol. A CT scan of the mouse lung was conducted 18 days after injecting the tumor cells to confirm the pulmonary tumorigenesis before the indicated therapy. Premixed M2pep-siYY1 was injected into the tail vein every 4 days at a dose of 15 mL/kg 20 days after injecting the tumor cells. InVivoMab anti-mouse PD-1 (CD279; BioXcell, Lebanon, NH, USA) was administered intraperitoneally every 4 days at 8 mg/kg 20 days after injecting the tumor cells. Changes in the pulmonary nodules were observed by re-examining the CT scans after the three injections. Six mice in each group were used for the survival analysis, and two mice in each group were sacrificed at the fifth week after tumor implantation to perform the pathological analysis of the lungs. The timeline is shown in online supplemental figure 1A.

Chromatin immunoprecipitation (ChIP) assay

The EpiQuik Plant ChIP Kit (Epigentek, Farmingdale, NY, USA) was used for the ChIP assay following the manufacturer's instructions. The THP-1 cells and induced M2 macrophages were cross-linked with 37% (v/v) formaldehyde for 10 min, treated with glycine for another 10 min to stop the reaction, and sonicated to 400–800 bp. Chromatin was then immunoprecipitated with YY1 and IgG antibodies on protein-A/G-agarose gel beads. The immunoprecipitated DNA was quantified using qRT-PCR after elution, cross-linking, and purification. The primer sequences for YY1, *p65*, and *CEBPB* are listed in online supplemental table 1.

Single-cell RNA sequencing data collection and analysis

The prostate single-cell RNA sequencing data set was obtained from a previous article.³⁹ The data contained paired tumor and normal samples from 10 patients. We applied the Seurat R package⁴⁷ for subsequent clustering, using the singleR package⁴⁸ based on published markers for cell annotation.

Transcription factor analysis and gene set variation analysis (GSVA)

To assess the strength of transcription factor regulation, we used pySCENIC (0.11.2)⁴⁹ to build the regulatory network of macrophages in both PCa and normal samples. Regulons were ranked by the difference in the regulon specificity score between tumor and normal tissue from high to low. The top 20 different regulons were used to plot the heatmap. Regulon specificity scores were scaled using the macrophage source. The GSVA R package (V.1.38.0) was used to estimate the pathway activity scores for the macrophages.⁵⁰ Differences in the pathway activity of macrophages between tumor and normal tissue were calculated using the limma R package (V.3.46.0).⁵¹

Identification of enhancers

The original reads were mapped to the human reference genome (GRCh37/hg19) using Bowtie2.⁵² To identify ChIP-seq peak regions, we performed peak calling using model-based analysis for ChIP-Seq (MACS) with the default parameters.⁵³ Finally, the peak regions of H3K27ac ChIP-seq data were used to determine the enhancer regions.

Phase separation droplet assay

The recombinant YY1-IDR (intrinsically disordered regions)–EGFP fusion protein was synthesized using GenScript (Piscataway, NJ, USA) and verified to be expressed in the *Escherichia coli* strains Rosetta 2 (DE3) and BL21 (DE3). The IDR and non-IDR segments of YY1 are shown in figure 8B, and the YY1-EGFP vector map is shown in online supplemental figure 6E. The recombinant protein (1 μ M) was desalted using potassium phosphate buffer at pH 7.0 and mixed with PEG8000 under different concentration gradients (5%, 10%, 20%, and 30%) as a molecule crowder. Different concentration gradients of the recombinant protein (1, 2, 5, 10, and 20 μ M) were then tested with 30% PEG8000. The mixed protein solution was loaded onto a glass slide with a coverslip and immediately visualized using a Fluoview FV1000 fluorescence confocal microscope (Olympus).

Fluorescence recovery after photobleaching (FRAP) assay

YY1-IDR-EGFP recombinant cells were transfected into THP-1 cell-derived macrophages. Fluoview FV3000 fluorescence confocal microscope (Olympus, Japan) was used for the FRAP assay. The photobleaching was performed using a 488 nm laser at 30% power, and a region with a radius of 1.5 μ m was defined as the targeted focus. Images were obtained every 10 s until 1 min after the photobleaching. ImageJ software was used to measure the



fluorescence intensities. Transfected macrophages were fixed and co-stained with 4',6-diamidino-2-phenylindole to determine the localization of the recombinant protein in the cells.

Statistical analysis

All experiments were independently repeated thrice, and Student's t-test or one-way ANOVA was used to compare the studied groups. Statistical results are presented as the mean±SD. All statistical analyses were performed using SPSS software V.16.0, and p value <0.05 indicated a statistically significant difference.

DISCUSSION

Although ICIs have a durable and favorable effect on tumor therapy, they only affect a subset of individuals with specific tumors.⁵⁴ The mechanisms of ICI failure include a low mutational burden,⁵⁵ effector T-cell deficiency or exhaustion,⁵⁶ and infiltration of immunosuppressive macrophages.^{57,58} PCa, a typical “cold” tumor, has an immunosuppressive microenvironment characterized by anti-tumoral T-lymphocyte deficiency and TAMs infiltration.⁶ TAMs inhibit the function of CD8⁺ cytotoxic T cells (CTLs) by secreting multiple cytokines and directly promoting the proliferation and invasion of tumor cells.⁵⁹ However, the therapeutic strategies targeting TAMs have not yet been sufficiently effective,⁶⁰ which may be related to the differentiation and function of both immunosuppressive M2 macrophage and tumor-suppressive M1 macrophage. Therefore, elucidating the tumor-promoting mechanism of M2 macrophage and precise targeting is essential for improving the therapeutic efficacy of immunotherapies targeting macrophages and immune checkpoints.

We generated a YY1 overexpressing transgenic mice model and found no noticeable abnormal morphological changes in multiple organs, including the reproductive system. However, the proportion of CD163⁺ M2 macrophages, including PCDMs and BMDMs, was significantly increased in YY1^{high} transgenic mice. Subsequently, subcutaneous tumors grew significantly faster in YY1^{high} transgenic mice than in control mice. We observed a significant increase in tumor-infiltrating CD163⁺ macrophages and a low infiltration of CD4⁺ and CD8⁺ T cells in subcutaneous tumors in YY1^{high} transgenic mice compared with that in control mice. To examine the therapeutic potential of targeting YY1 in M2 macrophages, M2pep-siYY1 was employed, and in vivo experiments showed that M2pep-siYY1 prolonged the survival of mice with PCa lung metastasis and had a synergistic effect with the PD-1 inhibitor. This research demonstrated that YY1-mediated macrophage infiltration in PCa leads to decreased proliferation and dysfunction of CD8⁺ and CD4⁺ T cells, the major target cell subgroups of ICIs.

YY1 can mutually regulate multiple cytokines, such as IL-6, IL-8, and IL-1β, which participate in the construction of TME.^{61–63} In this study, the expression of various

cytokines was decreased when YY1 was knocked down in M2 macrophages, among which IL-6 was the most significant. Further in vitro experiments demonstrated the effects of IL-6 on macrophage-induced PCa progression. Studies have shown that IL-6 can directly cause tumor cell progression by activating signaling pathways, such as STAT3 and NF-κB,^{64,65} but also inhibit Th1 differentiation of CD4⁺ helper T-cell and CD8⁺ cytotoxic T-cell (CTL) activation, resulting in impaired adaptive immune response and accelerated tumor proliferation and metastasis,⁶⁶ which can partly explain the specific mechanism of the synergistic anti-tumor effects of M2-targeted YY1 and PD-1 blockade.

Although some studies have reported that YY1 upregulated M2 macrophage markers in cardiac injury,⁶⁷ few studies have focused on the mechanisms of YY1 in M2 macrophages. This study showed that during M2 polarization of macrophages, IL-4/STAT6 transcriptionally upregulated YY1 and induced LLPS of YY1, increasing the interactions between the M2-specific IL-6 enhancer and promoter. Phase separation is a physicochemical process in which multiple mixtures are separated and aggregated into droplets of different phases. TFs can form liquid-phase-separated aggregates on enhancer clusters under the action of the IDRs; thus, TFs with synergistic functions can be aggregated and localized to promote gene transcription.^{30,68,69} This phenomenon clarifies the mechanism by which YY1 forms a transcriptional complex with p300/p65/CEBPB to promote IL-6 transcription.

YY1 promotes the interaction between the active enhancer and promoter by forming dimers, while deletion of YY1 could disrupt the enhancer-promoter looping.³¹ YY1 can also stimulate oncogene expression through p300-mediated histone acetylation,⁷⁰ a marker of active enhancers and a key component in the identified YY1 complex. Therefore, we conducted ChIP-seq of M2 macrophages and THP-1 cells. The significantly increased H3K27ac and YY1 signals identified a fragment of the M2-specific enhancer, increasing the protumorigenic ability of M2 macrophages. In addition, inhibitors of the YY1 complex or the enhancers were used to disrupt the transcription complex, and the progression of mouse PCa was suppressed. Consistent with our results, a recent study reported that YY1 promoted phase separation condensates to compartmentalize enhancers and coactivators, including p300, BRD4, and MED1, thus activating downstream gene expression.⁷¹ Here, for the first time, we identified the role of p65 and CEBPB in YY1-mediated phase separation and clarified that the phase separation of YY1 participates in M2 macrophage polarization and function. However, YY1 and coactivators are involved in multiple biological processes. Therefore, further studies are still necessary to determine whether cancer patients can benefit from targeted therapies.

In addition, although YY1 contains a relatively long IDR required for phase separation, the non-IDR segment remains the primary region for DNA binding.⁷² Herein, we showed that YY1-IDR was the key domain mediating

LLPS in M2 macrophages. According to the spatial structure prediction, the coactivators p300, p65, and CEBPB in the YY1 complex were mainly combined with YY1-IDR, which was also confirmed by the immunoprecipitation of YY1-IDR-EGFP. The expression of downstream IL-6 and M2 macrophage markers was also significantly inhibited by YY1-IDR knockout. These results suggest that YY1-IDR plays a central role in YY1-mediated M2 macrophage polarization and PCa progression. The potential therapeutic strategy of targeting YY1-IDR may relieve the immunosuppressive TME caused by YY1 while retaining its normal physiological function.

In conclusion, we have provided a landscape of the YY1 expression and a YY1-mediated regulatory network in M2 macrophages in PCa. We used *in vitro* and transgenic mice experiments to show that YY1 participated in M2 macrophage polarization and exerted pro-tumor function in PCa. Mechanistically, IL-4/STAT6 transcriptionally upregulated YY1 and induced LLPS of YY1, increasing the interaction between M2-specific IL-6 enhancer and promoter. These findings provide a rationale for further research and development of therapies targeting YY1 in macrophages in the TME of PCa.

Author affiliations

¹Department of Urology, Southeast University Zhongda Hospital, Nanjing, Jiangsu, China

²Surgical Research Center, Institute of Urology, Southeast University Medical School, Nanjing, China

³Key Laboratory of Biomedical Information Engineering of Ministry of Education, Biomedical Informatics & Genomics Center, School of Life Science and Technology, Xi'an Jiaotong University, Xi'an, China

⁴Department of Bioinformatics, School of Biomedical Engineering and Informatics, Nanjing Medical University, Nanjing, Jiangsu, China

⁵Department of Pathology, Southeast University Zhongda Hospital, Nanjing, China

⁶School of Biomedical Sciences, Hunan University, Changsha, Hunan, China

⁷Department of Radiology, Southeast University Zhongda Hospital, Nanjing, China

⁸Institute of Medical Phenomics Research, Southeast University Zhongda Hospital, Nanjing, Jiangsu, China

Acknowledgements We are grateful to the staff of the Public Scientific Research Platform of Zhongda Hospital affiliated with Southeast University, and the Scientific Research Sharing Platform of Southeast University Medical school, for technical assistance.

Contributors BX and MC conceived, designed, and supervised the study. WL and SaC performed the experiments and wrote the original draft of the manuscript with help from DZ, ZY, KL and TW collected the data and interpreted the results. YH and CS analyzed the data and proofread the manuscript. XW and LZ provided pathology expertise. SJ, DZ and GZ provided material and technical support. ShC, JW and NS provided and collected the clinical samples. BX, as the guarantor, accepts full responsibility for the work and the conduct of the study.

Funding The authors disclosed receipt of the following financial support for the research, authorship, and/or publication of this article. This work was supported by the National Natural Science Foundation of China (grant numbers 81872089, 82102799, 82203685), Natural Science Foundation of Jiangsu Province (grant number BK20210230), Jiangsu Provincial Key Research and Development Program (grant number BE2019751), Natural Science Basic Research Program of Shaanxi (grant number 2021JQ-023), Doctor of Entrepreneurship and Innovation in Jiangsu Province (grant number JSSCBS20210088, JSSCBS20210138) and The General Project of Medical Research of Jiangsu Health and Wellness Committee (grant number M2020049).

Competing interests None declared.

Patient consent for publication Consent obtained directly from patient(s).

Ethics approval This study involves human participants and the study design was approved by the Ethics Committee of Zhongda Hospital Southeast University. The approval ID is 2022ZDKYSB099. All human tumor tissue samples were collected in accordance with the national and institutional ethical guidelines. Participants gave informed consent to participate in the study before taking part.

Provenance and peer review Not commissioned; externally peer reviewed.

Data availability statement All data relevant to the study are included in the article or uploaded as online supplemental information. The supporting data and materials are provided in online supplemental information. YY1 and H3K27ac ChIP-seq data sets for M2 and THP-1 cell lines and RNA-seq data for oe/nc-YY1 M2 macrophages CM-treated LNCaP are available at the GEO repository under accession GSE200949.

Supplemental material This content has been supplied by the author(s). It has not been vetted by BMJ Publishing Group Limited (BMJ) and may not have been peer-reviewed. Any opinions or recommendations discussed are solely those of the author(s) and are not endorsed by BMJ. BMJ disclaims all liability and responsibility arising from any reliance placed on the content. Where the content includes any translated material, BMJ does not warrant the accuracy and reliability of the translations (including but not limited to local regulations, clinical guidelines, terminology, drug names and drug dosages), and is not responsible for any error and/or omissions arising from translation and adaptation or otherwise.

Open access This is an open access article distributed in accordance with the Creative Commons Attribution Non Commercial (CC BY-NC 4.0) license, which permits others to distribute, remix, adapt, build upon this work non-commercially, and license their derivative works on different terms, provided the original work is properly cited, appropriate credit is given, any changes made indicated, and the use is non-commercial. See <http://creativecommons.org/licenses/by-nc/4.0/>.

ORCID iD

Bin Xu <http://orcid.org/0000-0003-4993-0500>

REFERENCES

- Culp MB, Soerjomataram I, Efsthathiou JA, *et al.* Recent global patterns in prostate cancer incidence and mortality rates. *Eur Urol* 2020;77:38–52.
- Siegel RL, Miller KD, Fuchs HE, *et al.* Cancer statistics, 2022. *CA Cancer J Clin* 2022;72:7–33.
- Sehrawat A, Gao L, Wang Y, *et al.* LSD1 activates a lethal prostate cancer gene network independently of its demethylase function. *Proc Natl Acad Sci U S A* 2018;115:E4179–88.
- Graff JN, Beer TM, Alumkal JJ, *et al.* A phase II single-arm study of pembrolizumab with enzalutamide in men with metastatic castration-resistant prostate cancer progressing on enzalutamide alone. *J Immunother Cancer* 2020;8:e000642.
- Hanahan D, Weinberg RA. Hallmarks of cancer: the next generation. *Cell* 2011;144:646–74.
- Wu Z, Chen H, Luo W, *et al.* The landscape of immune cells infiltrating in prostate cancer. *Front Oncol* 2020;10:517637.
- Solinas G, Germano G, Mantovani A, *et al.* Tumor-associated macrophages (TAM) as major players of the cancer-related inflammation. *J Leukoc Biol* 2009;86:1065–73.
- Guo Q, Li X, Zhou W, *et al.* Sequentially triggered bacterial outer membrane vesicles for macrophage metabolism modulation and tumor metastasis suppression. *ACS Nano* 2021;15:13826–38.
- Chen S, Zhu G, Yang Y, *et al.* Single-cell analysis reveals transcriptomic remodellings in distinct cell types that contribute to human prostate cancer progression. *Nat Cell Biol* 2021;23:87–98.
- Schroder K, Sweet MJ, Hume DA. Signal integration between IFN γ and TLR signalling pathways in macrophages. *Immunobiology* 2006;211:511–24.
- Yang L, Zhang Y. Tumor-associated macrophages: from basic research to clinical application. *J Hematol Oncol* 2017;10:58.
- Song M, Yeku OO, Rafiq S, *et al.* Tumor derived UBR5 promotes ovarian cancer growth and metastasis through inducing immunosuppressive macrophages. *Nat Commun* 2020;11:6298.
- Jahchan NS, Mujal AM, Pollack JL, *et al.* Tuning the tumor myeloid microenvironment to fight cancer. *Front Immunol* 2019;10:1611.
- Qian BZ, Pollard JW. Macrophage diversity enhances tumor progression and metastasis. *Cell* 2010;141:39–51.
- Yang M, McKay D, Pollard JW, *et al.* Diverse functions of macrophages in different tumor microenvironments. *Cancer Res* 2018;78:5492–503.

- 16 Atchison M, Basu A, Zaprazna K, *et al.* Mechanisms of yin yang 1 in oncogenesis: the importance of indirect effects. *Crit Rev Oncog* 2011;16:143–61.
- 17 Wu S, Wang H, Li Y, *et al.* Transcription factor YY1 promotes cell proliferation by directly activating the pentose phosphate pathway. *Cancer Res* 2018;78:4549–62.
- 18 Gordon S, Akopyan G, Garban H, *et al.* Transcription factor YY1: structure, function, and therapeutic implications in cancer biology. *Oncogene* 2006;25:1125–42.
- 19 Zhou X, Xian W, Zhang J, *et al.* YY1 binds to the E3' enhancer and inhibits the expression of the immunoglobulin κ gene via epigenetic modifications. *Immunology* 2018;155:491–8.
- 20 Deng Z, Cao P, Wan MM, *et al.* Yin yang 1: a multifaceted protein beyond a transcription factor. *Transcription* 2010;1:81–4.
- 21 He Y, Casaccia-Bonnell P. The yin and yang of YY1 in the nervous system. *J Neurochem* 2008;106:1493–502.
- 22 Krippner-Heidenreich A, Walsemann G, Beyrouthy MJ, *et al.* Caspase-dependent regulation and subcellular redistribution of the transcriptional modulator YY1 during apoptosis. *Mol Cell Biol* 2005;25:3704–14.
- 23 van Leenders GJLH, Dukers D, Hessels D, *et al.* Polycomb-group oncogenes EZH2, BMI1, and RING1 are overexpressed in prostate cancer with adverse pathologic and clinical features. *Eur Urol* 2007;52:455–63.
- 24 Huang Y, Tao T, Liu C, *et al.* Upregulation of miR-146a by YY1 depletion correlates with delayed progression of prostate cancer. *Int J Oncol* 2017;50:421–31.
- 25 Jian D, Dai B, Hu X, *et al.* Ox-Ldl increases microRNA-29a transcription through upregulating YY1 and STAT1 in macrophages. *Cell Biol Int* 2017;41:1001–11.
- 26 Su K, Li X, Edberg JC, *et al.* A promoter haplotype of the immunoreceptor tyrosine-based inhibitory motif-bearing Fc γ RIIB alters receptor expression and associates with autoimmunity. II. Differential binding of GATA4 and yin-yang1 transcription factors and correlated receptor expression and function. *J Immunol* 2004;172:7192–9.
- 27 Tang Y, Wang D, Niu X, *et al.* Mild iron overload induces TRIP12-mediated degradation of YY1 to trigger hepatic inflammation. *Free Radic Biol Med* 2020;161:187–97.
- 28 Zhang X, Liu J, Wu L, *et al.* MicroRNAs of the mir-17–9 family maintain adipose tissue macrophage homeostasis by sustaining IL-10 expression. *Life* 2020;9:e55676.
- 29 Bojja A, Klein IA, Sabari BR, *et al.* Transcription factors activate genes through the phase-separation capacity of their activation domains. *Cell* 2018;175:1842–55.
- 30 Sabari BR, Dall'Agnese A, Bojja A, *et al.* Coactivator condensation at super-enhancers links phase separation and gene control. *Science* 2018;361:361.
- 31 Weintraub AS, Li CH, Zamudio AV, *et al.* YY1 is a structural regulator of enhancer-promoter loops. *Cell* 2017;171:1573–88.
- 32 Sarvagalla S, Kolapalli SP, Vallabhapurapu S. The two sides of YY1 in cancer: a friend and a foe. *Front Oncol* 2019;9:1230.
- 33 Cieslewicz M, Tang J, Yu JL, *et al.* Targeted delivery of proapoptotic peptides to tumor-associated macrophages improves survival. *Proc Natl Acad Sci U S A* 2013;110:15919–24.
- 34 Han J, Meng J, Chen S, *et al.* Yy1 complex promotes quaking expression via super-enhancer binding during EMT of hepatocellular carcinoma. *Cancer Res* 2019;79:1451–64.
- 35 Wang Y-C, Wu Y-S, Hung C-Y, *et al.* USP24 induces IL-6 in tumor-associated microenvironment by stabilizing p300 and β -trcp and promotes cancer malignancy. *Nat Commun* 2018;9:3996.
- 36 Baylin SB, Jones PA. A decade of exploring the cancer epigenome: biological and translational implications. *Nat Rev Cancer* 2011;11:726–34.
- 37 Ahuja N, Easwaran H, Baylin SB. Harnessing the potential of epigenetic therapy to target solid tumors. *J Clin Invest* 2014;124:56–63.
- 38 Wang J, Wu X, Wei C, *et al.* YY1 positively regulates transcription by targeting promoters and super-enhancers through the BAF complex in embryonic stem cells. *Stem Cell Reports* 2018;10:1324–39.
- 39 Tuong ZK, Loudon KW, Berry B, *et al.* Resolving the immune landscape of human prostate at a single-cell level in health and cancer. *Cell Rep* 2021;37:110132.
- 40 Wilson MR, Reske JJ, Holladay J, *et al.* ARID1A mutations promote p300-dependent endometrial invasion through super-enhancer hyperacetylation. *Cell Rep* 2020;33:108366.
- 41 Tsang FH-C, Law C-T, Tang T-CC, *et al.* Aberrant super-enhancer landscape in human hepatocellular carcinoma. *Hepatology* 2019;69:2502–17.
- 42 Tan Y, Wang X, Song H, *et al.* A PML/rar α direct target atlas redefines transcriptional deregulation in acute promyelocytic leukemia. *Blood* 2021;137:1503–16.
- 43 Lai B, Lee JE, Jang Y, *et al.* MLL3/MLL4 are required for CBP/p300 binding on enhancers and super-enhancer formation in brown adipogenesis. *Nucleic Acids Res* 2017;45:6388–403.
- 44 Tasdemir N, Banito A, Roe JS, *et al.* BRD4 connects enhancer remodeling to senescence immune surveillance. *Cancer Discov* 2016;6:612–29.
- 45 Liu J, Duan Z, Guo W, *et al.* Targeting the BRD4/foxo3a/CDK6 axis sensitizes akt inhibition in luminal breast cancer. *Nat Commun* 2018;9:5200.
- 46 Donati B, Lorenzini E, Ciarrocchi A. BRD4 and cancer: going beyond transcriptional regulation. *Mol Cancer* 2018;17:164:164..
- 47 Stuart T, Butler A, Hoffman P, *et al.* Comprehensive integration of single-cell data. *Cell* 2019;177:S0092-8674(19)30559-8:1888–1902..
- 48 Aran D, Looney AP, Liu L, *et al.* Reference-based analysis of lung single-cell sequencing reveals a transitional profibrotic macrophage. *Nat Immunol* 2019;20:163–72.
- 49 Aibar S, González-Blas CB, Moerman T, *et al.* SCENIC: single-cell regulatory network inference and clustering. *Nat Methods* 2017;14:1083–6.
- 50 Hänzelmann S, Castelo R, Guinney J. GSEA: gene set variation analysis for microarray and RNA-Seq data. *BMC Bioinformatics* 2013;14:7.
- 51 Ritchie ME, Phipson B, Wu D, *et al.* Limma powers differential expression analyses for RNA-sequencing and microarray studies. *Nucleic Acids Res* 2015;43:e47.
- 52 Langmead B, Salzberg SL. Fast gapped-read alignment with Bowtie 2. *Nat Methods* 2012;9:357–9.
- 53 Zhang Y, Liu T, Meyer CA, *et al.* Model-based analysis of ChIP-Seq (MACS). *Genome Biol* 2008;9:R137.
- 54 Jenkins RW, Barbie DA, Flaherty KT. Mechanisms of resistance to immune checkpoint inhibitors. *Br J Cancer* 2018;118:9–16.
- 55 Le DT, Durham JN, Smith KN, *et al.* Mismatch repair deficiency predicts response of solid tumors to PD-1 blockade. *Science* 2017;357:409–13.
- 56 Miller BC, Sen DR, Al Abosy R, *et al.* Subsets of exhausted CD8+ T cells differentially mediate tumor control and respond to checkpoint blockade. *Nat Immunol* 2019;20:326–36.
- 57 Dammeijer F, Lievense LA, Kaijen-Lambers ME, *et al.* Depletion of tumor-associated macrophages with a CSF-1R kinase inhibitor enhances antitumor immunity and survival induced by DC immunotherapy. *Cancer Immunol Res* 2017;5:535–46.
- 58 Dannenmann SR, Thielicke J, Stöckli M, *et al.* Tumor-associated macrophages subvert T-cell function and correlate with reduced survival in clear cell renal cell carcinoma. *Oncol Immunology* 2013;2:e23562.
- 59 Peranzoni E, Lemoine J, Vimeux L, *et al.* Macrophages impede CD8 T cells from reaching tumor cells and limit the efficacy of anti-PD-1 treatment. *Proc Natl Acad Sci USA* 2018;115:E4041–50.
- 60 Nywening TM, Wang-Gillam A, Sanford DE, *et al.* Targeting tumour-associated macrophages with CCR2 inhibition in combination with folirinox in patients with borderline resectable and locally advanced pancreatic cancer: a single-centre, open-label, dose-finding, non-randomised, phase 1B trial. *Lancet Oncol* 2016;17:651–62.
- 61 Wang H, Garzon R, Sun H, *et al.* NF-kappab-YY1-mir-29 regulatory circuitry in skeletal myogenesis and rhabdomyosarcoma. *Cancer Cell* 2008;14:369–81.
- 62 Zhang Y, He S, Mei R, *et al.* MiR-29a suppresses il-13-induced cell invasion by inhibiting YY1 in the Akt pathway in lung adenocarcinoma A549 cells. *Oncol Rep* 2018;39:2613–23.
- 63 Lai C-Y, Lin C-Y, Hsu C-C, *et al.* Liver-directed microRNA-7a depletion induces nonalcoholic fatty liver disease by stabilizing YY1-mediated lipogenic pathways in zebrafish. *Biochim Biophys Acta Mol Cell Biol Lipids* 2018;1863:844–56.
- 64 Iliopoulos D, Hirsch HA, Struhl K. An epigenetic switch involving NF-kappaB, Lin28, let-7 microRNA, and IL6 links inflammation to cell transformation. *Cell* 2009;139:693–706.
- 65 Li L, Yu R, Cai T, *et al.* Effects of immune cells and cytokines on inflammation and immunosuppression in the tumor microenvironment. *Int Immunopharmacol* 2020;88:106939.
- 66 Tsukamoto H, Fujieda K, Senju S, *et al.* Immune-suppressive effects of interleukin-6 on T-cell-mediated anti-tumor immunity. *Cancer Sci* 2018;109:523–30.
- 67 Huang Y, Li L, Chen H, *et al.* The protective role of yin-yang 1 in cardiac injury and remodeling after myocardial infarction. *J Am Heart Assoc* 2021;10:e021895.
- 68 Cho W-K, Spille J-H, Hecht M, *et al.* Mediator and RNA polymerase II clusters associate in transcription-dependent condensates. *Science* 2018;361:412–5.

- 69 Tsang B, Pritišanac I, Scherer SW, *et al.* Phase separation as a missing mechanism for interpretation of disease mutations. *Cell* 2020;183:1742–56.
- 70 Baumeister P, Luo S, Skarnes WC, *et al.* Endoplasmic reticulum stress induction of the grp78/BiP promoter: activating mechanisms mediated by YY1 and its interactive chromatin modifiers. *Mol Cell Biol* 2005;25:4529–40.
- 71 Wang W, Qiao S, Li G, *et al.* A histidine cluster determines YY1-compartmentalized coactivators and chromatin elements in phase-separated enhancer clusters. *Nucleic Acids Res* 2022;50:4917–37.
- 72 Brodsky S, Jana T, Mittelman K, *et al.* Intrinsically disordered regions direct transcription factor in vivo binding specificity. *Molecular Cell* 2020;79:459–471.